Fall 11-4-2016

Abrupt Ocean Anoxia During the Late Ordovician Mass Extinction Detected Using Uranium Isotopes of Marine Carbonates

Rickey Bartlett
University of New Mexico

Maya Elrick
University of New Mexico

Yemane Asmerom
University of New Mexico

Viorel Atudorei
University of New Mexico

Rickey Bartlett

Candidate

Earth and Planetary Sciences

Department

This thesis is approved, and it is acceptable in quality and form for publication:

Approved by the thesis committee:

Dr. Maya Elrick, Earth and Planetary Sciences, chairperson

Dr. Yemane Asmerom, Earth and Planetary Sciences

Dr. Viorel Atudorei, Earth and Planetary Sciences

ABRUPT OCEAN ANOXIA DURING THE LATE ORDOVICIAN MASS EXTINCTION DETECTED USING URANIUM ISOTOPES OF MARINE CARBONATES

BY

RICKEY BARTLETT

B.S., GEOLOGY, NORTHERN ARIZONA UNIVERSITY, 2011

THESIS

Submitted in Partial Fulfillment of the
Requirements for the Degree of

Master of Science
Earth and Planetary Sciences

The University of New Mexico
Albuquerque, New Mexico

December, 2016

ABRUPT OCEAN ANOXIA DURING THE LATE ORDOVICIAN MASS EXTINCTION DETECTED USING URANIUM ISOTOPES OF MARINE CARBONATES

by

Rickey Bartlett

B.S., Geology, Northern Arizona University, 2011

ABSTRACT

The Ordovician witnessed an explosion in marine biodiversity punctuated by the first of the 'big-5' Phanerozoic mass extinctions, the Late Ordovician mass extinction (LOME). The LOME consists of two discrete pulses occurring at the beginning and end of the Hirnantian. Lithologic and geochemical evidence suggests widespread marine anoxia triggered the second LOME pulse; however, most of these redox proxies record local bottom water or porewater conditions rather than global seawater conditions. To evaluate global redox trends, we utilize uranium (U) isotopes and trace element geochemistry of marine carbonates as a global marine redox proxy.

Bulk carbonate samples were collected from the upper Katian, Hirnantian, and through the lowermost Rhuddanian on Anticosti Island, Quebec with a focus on the second LOME pulse. We target this specific location because the U-isotope seawater redox proxy can be directly compared to the well documented, high-resolution record of glacio-eustasy, Hirnantian positive carbon isotope excursion (HICE), and faunal diversity trends

previously reported from Anticosti Island which removes any potential temporal mismatches among proxy records.

Measured $\delta^{238}U$ values range from -0.83 ‰ to 0.44 ‰ with values averaging ~ -0.25 ‰ in the late Katian through late Hirnantian indicating more oxic conditions, an abrupt (<20 ky) -0.35 ‰ negative shift lasting ~450 ky representing more reducing conditions, followed by an abrupt positive shift back to values averaging ~0.25 in the earliest Silurian (early Rhuddanian). Th/U values average ~0.8 during the late Katian to late Hirnantian and shift to an average of ~2.2 in the late Hirnantian before returning to an average of ~1. Total organic carbon (TOC) values are low (average = 0.19%) for the entire section with a brief increase in the latest Hirnantian. Combined, these proxies indicate a global record of an abrupt latest Hirnantian oceanic anoxic event (HOAE) during the Late Ordovician icehouse. Simple box modeling of the event suggests that there was a ~7x increase in anoxic sediment deposition and U sequestration to generate the observed shift and the rapidity of the onset implies that Latest Ordovician oceans had significantly lower U concentrations than modern oceans.

The HOAE onset is coincident with the LOME onset but lasted ~200 ky longer, suggesting anoxic conditions did not affect the biologic recovery. The HOAE began during the deglacial highstand before peak glaciation and persisted through the peak glacial lowstand and subsequent deglacial rise, which indicates water depths and shoreline positions did not influence anoxic sediment accumulation. The largest HICE peak occurs during the HOAE but is not coincident with its onset and demise, indicating the processes controlling $\delta^{13}C$ trends were partially decoupled with anoxic sediment deposition.

We propose that the HOAE was the result of global cooling, more vigorous thermohaline circulation and upwelling, increased nutrient delivery and enhanced primary productivity which resulted in an expanded oxygen minimum zone and anoxic sediment deposition. This icehouse-related model contrasts with those proposed for other Phanerozoic OAEs, which developed under greenhouse climate conditions.

TABLE OF CONTENTS

1. INTRODUCTION……1

2. GEOLOGIC AND GEOCHEMICAL BACKGROUND……2

2.1. Anoxia and Euxinia in the Ocean……2

2.2. Ordovician paleoclimate and paleogeography……4

2.3. The GOBE……6

2.4. The LOME……7

2.5. Anticosti Island……9

2.6. Late Ordovician marine anoxia……10

2.7. Uranium isotope systematics……11

3. MATERIALS AND METHODS……14

4. RESULTS……15

5. DISCUSSION……17

5.1. Evidence for primary signal……17

5.2. Correction for contribution from anoxic porewater derived cements……19

6. LATE HIRNANTIAN ANOXIA……20

6.1. The Hirnantian OAE……20

6.2. The HOAE and its relationship to the HICE……22

6.3. Comparison to other OAEs……23

7. HOAE MODEL……23

7.1. Contributing causes?……27

8. CONCLUSIONS……27

SUPPLIMENTAL MATERIALS……29

REFERENCES……43

1. Introduction

The Middle to Late Ordovician records significant paleoenvironmental events including a greenhouse to icehouse climatic transition, extensive continental glaciation (peaking in the Hirnantian) and associated glacio-eustatic sea-level changes despite estimated high atmospheric CO_2 levels (Yapp and Poths, 1992; Berner and Kothavala, 2001), a major biologic diversity increase punctuated by the first of the 'big five' mass extinctions (Late Ordovician mass extinction or LOME), and a significant perturbation in the global carbon cycle indicated by the Hirnantian positive carbon isotope excursion (HICE) (Droser and Finnegan, 2003; Harper, 2006; Servais et al., 2010; Ghienne et al., 2014). The LOME eradicated up to 85% of marine species and occurred in two discrete pulses, one at the beginning of the Hirnantian and the other about 1.5 My later at the end of the Hirnantian (Brenchley, 1994; Sheehan, 2001; Finnegan et al., 2011). The first pulse has been attributed to glacio-eustatic sea-level fall and loss of shallow-marine habitats (Berry and Wilde, 1978; Brenchley, 1994; Finnegan et al, 2012); however, this interpretation has been recently challenged and is now documented to have occurred during a melting phase (Ghienne et al., 2014). The origin of the second pulse, which is the focus of this study, is most commonly attributed to widespread marine anoxia (Brenchley et al., 2003; Harper et al., 2013). Data for this interpretation comes from a range of sedimentologic and geochemical records; however, the majority of these redox proxies only evaluate local bottom water or porewater conditions and the redox signals are derived from geographically separated locations so that the timing relationships among major biologic and other paleoenvironmental events are not well constrained.

To develop a global marine redox curve across the LOME and to alleviate potential timing mismatches among associated climatic, biologic, and geochemical events, we utilize U isotopes of Upper Ordovician marine carbonates from western Anticosti Island, Canada. We target this specific location because previous studies document 1) a clear glacio-eustatic record which tracks the history of orbitally controlled continental glaciation (Ghienne et al., 2014), 2) a detailed and stratigraphically expanded $\delta^{13}C$ curve, 3) faunal diversity trends which identify the LOME pulses, and 4) robust age control from chitinozoa. We utilize U isotopes of marine carbonates because the marine residence time of U is significantly longer than ocean mixing times and seawater U-isotope fractionation occurs during the reduction and sequestration of U^{4+} into anoxic sediments (Chen et al., 1986; Dunk et al., 2002; Romaniello et al., 2013; Tissot and Dauphas, 2015).

The specific objectives of this study are to: 1) describe and interpret U-isotope and trace element trends across the LOME, with a focus on the second extinction pulse, and 2) correlate and interpret relationships among anoxia and other previously reported Late Ordovician paleoenvironmental events to better understand the development of widespread marine anoxia during an icehouse climate.

2. Geologic and Geochemical Background

2.1. Anoxia and Euxinia in the Ocean

Modern oceans, while strongly stratified, are well oxygenated, but this has not always been the case. For long periods of Earth's history, anoxic/euxinic conditions may have been prevalent (Canfield, 1998). Anoxia arises when oxygen is consumed by biological or chemical processes more

rapidly than it is either created or imported. When this occurs, organisms must turn to other electron recipients such as trace metals and nitrates. These sources are limited and eventually depleted, at which point sulfate reduction begins resulting in high levels of free hydrogen sulfide and a toxic condition referred to as euxinia (Meyer and Kump, 2008).

Anoxia in the ocean can be promoted in a variety of ways. During warm periods, the oxygen concentrations of the oceans drop due to the lower solubility of oxygen in warmer waters. Such a decrease can either directly drive anoxia or increase the likelihood of it being produced by other factors (Schlanger and Jenkyns, 1976; Fischer and Arthur, 1977; Hotinski et al., 2001). Secondly, an increase in primary productivity within the photic-zone leads to a corresponding increase in the biomass available in the water column; the inevitable decomposition of this organic material beneath the zone of primary production consumes available oxygen, thus producing an expansion of the oxygen minimum zone (OMZ) associated with the primary production. If the OMZ intersects the seafloor, this leads to a corresponding increase in deposition occurring under anoxic conditions (Fig. S1a). Given a continental shelf configuration with a very low gradient, a relatively small expansion increase in the vertical dimensions of the OMZ could greatly increase the area of deposition occurring under anoxic/euxinic conditions.

A geographic configuration that promotes deposition under anoxic conditions is one that favors the formation of restricted basins (Fig. S1b). Such basins serve as very efficient nutrient traps which allow for complete utilization of available nutrients with limited exchange with the world's oceans (Meyer and Kump, 2008). This increase in the efficient use of limiting nutrients within a given geographic area can lead to the complete consumption of available oxygen via decomposition, resulting in local

anoxic/euxinic conditions. If such nutrient trapping does provide a possible mechanism for driving the prevalence of deposition under anoxic/euxinic conditions, then this provides a possible link between changing sea levels and such conditions.

A third, though perhaps less plausible, means of increasing the prevalence of deposition occurring under anoxic conditions is significant reduction of deep ocean circulation (Fig. S1c). It has often been suggested that stagnation or very sluggish ocean circulation can promote anoxic conditions; this view is informed by conditions in the modern Black Sea, however, this is not a valid analog (Arthur and Sageman, 1994) for the global oceans. Under conditions of reduced circulation, consumption of oxygen will be greatly diminished due to limited nutrient cycling (Hotinski et al., 2001). Deep water oxygen levels under such conditions are likely to be reduced but are not likely to become anoxic or euxinic. Even in the most extreme cases of complete thermal and haline homogeneity in the oceans, heat flow from the sea floor would force overturning and mix the oceans on a 15,000 year time scale (Worthington, 1968).

2.2. Ordovician paleoclimate and paleogeography

Late Ordovician paleogeography is dominated by the wide spatial distribution of continents with Laurentia, Siberia and Baltica straddling the paleo-equator and the southern supercontinent of Gondwana spanning from the southern pole to ~10^{o} N (Fig. 1). The Ordovician records the transition from a long-term greenhouse to an icehouse climate with cooling beginning in the Early Ordovician, stabilization in the Middle Ordovician, then abrupt cooling and peak glacial conditions in the Latest Ordovician (Hirnantian) (Veizer et al., 2000; Shields et al., 2003; Kasting et al., 2006; Trotter et al.,

2008). Warming and deglaciation began in the Early Silurian (Rhuddanian) and continued into the Middle Silurian (Finnegan et al., 2011). Global sea levels were high throughout most of the Ordovician, generating vast epeiric seas and abundant shallow marine habitats. Estimated pCO_2 levels were many times higher than modern levels (Yapp and Poths, 1992; bi and Kothavala, 2001; Berner 2006; Nardin et al., 2011) despite clear evidence of major continental glaciation centered in northern Africa. How glaciation could occur with such high pCO_2 is debated, though it is possible that a dimmer sun, ~5% less than modern luminosity (Sheehan, 2001, 2001a), could have offset some of the warming effect of the high CO_2 levels. Others have suggested an increase in continental weathering driven by the Taconic Orogeny could cause a decline in atmospheric CO_2 due to the increased weathering of silicate minerals (Harper et al., 2013). The lowering of atmospheric CO_2 would lead to global cooling and initiation of southern glaciation and falling sea-levels. The 'weathering hypothesis' has the added benefit of explaining the $\delta^{13}C$ excursion observed at this time in terms of an increase in the weathering of exposed carbonate platforms. Some have also suggested widespread terrestrial flora (Lenton et al., 2012) as an explanation for cooling.

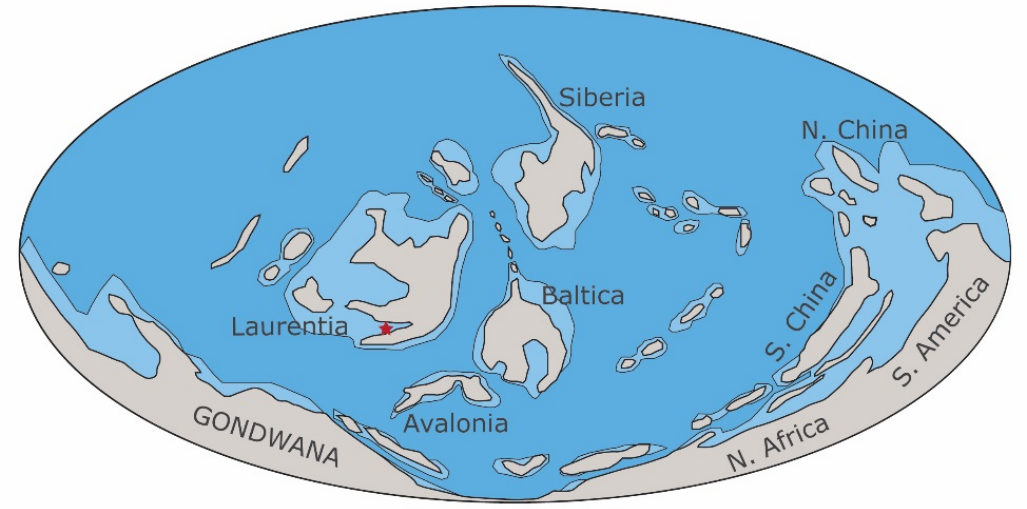

Fig. 1. Paleogeographical reconstruction of the Late Ordovician. Adapted from reconstructions by Blakey (http://cpgeosystems.com/index.html). Red star denotes the location of study area on Anticosti Island, Canada.

2.3. The GOBE

There have been two major increases in marine biodiversity during the Phanerozoic, the first during the early Paleozoic and the second during the Mesozoic (Sheehan, 2001a; Stanley, 2007; Servais and Owen, 2010). The early Paleozoic expansion in marine biodiversity consists of the "Cambrian Explosion" and the "Great Ordovician Biodiversification Event" or GOBE.

The GOBE features an explosion in marine biodiversity with an increase in metazoan diversity and a substantial increase in biocomplexity with the advent of metazoan reefs, increased predation, greater phytoplankton diversity and more complex food webs (Droser and Finnegan, 2003; Harper, 2006; Servais et al., 2010). The GOBE also marks the rise of both the Paleozoic and Modern Evolutionary Faunas while the Cambrian Evolutionary Faunas decline, never to recover (Sheehan, 2001).

Many ideas regarding the drivers for the GOBE have been suggested with no single definitive explanation winning out; however, it is most likely that it represented a coincidence of favorable continental configurations, favorable ocean temperatures (cooling from Cambrian hothouse conditions) and available tropical shallow marine habitat due to globally high sea levels for most of the Ordovician (Trotter et al., 2008; Servais et al., 2010). It is also possible that the GOBE and the Cambrian Explosion actually represent one interconnected and continuous radiation event (Droser and Finnegan, 2003) beginning during the Cambrian. The separation into two distinct stages may merely be a sampling artifact (Nardin and Lefebvre, 2010). In this 'single event' view, the Cambrian-GOBE radiation can be thought of as beginning with the advent of metazoans during the Ediacaran, then the development of hard body parts during the late Neoproterozoic and Early Cambrian, followed by

massive experimentation with various body plans during the Early to Middle Cambrian. During the Ordovician the most successful body plans undergo an explosive increase in diversity at the family, genus and species levels along with an accompanying complexity among communities. This increase in complexity leads to the expansion of metazoan communities into the deep sea as well as the development of reef and mudmound complexes (Harper, 2006; Harper et al., 2013).

2.4. The LOME

The expansion represented by the GOBE is punctuated by the first of the 'big-five' Phanerozoic mass extinctions, the Late Ordovician Mass Extinction (LOME). The LOME resulted in the loss of 85% of all marine species and 25% of animal families (Fig. S2; Sepkoski, 1996; Jablonski, 1991) with the majority of the losses occurring at lower taxonomic levels with no loss or replacement of higher taxa (Rasmussen and Harper, 2011). The LOME is unique among the 'big-five' and other Phanerozoic extinctions in that it is associated with glaciation; there is no other evidence during the Phanerozoic of glaciation having a significant effect on bio-diversity with the possible exception of the Mississippian Serpukhovian extinction event (McGhee et al., 2012). Many mechanisms have been suggested as the cause of the LOME: cooling and habitat loss, amalgamation of the continents leading to reduced and altered ecospace, deep-water anoxia due to ocean stagnation, encroachment of deep, anoxic waters onto the continental shelf, increased oxygenation of deep waters, widespread volcanism, bolide impact as well as gamma-ray bursters have all been implicated (Melott et al., 2004; Melott and Thomas, 2009; Stanley and Powell, 2003; Stanley, 2010; McGhee et al., 2012; Vandenbroucke et al., 2010; Finnegan et al., 2012; Hammarlund et al., 2012; Berry et al., 1990; Brenchley, 2001; Sheehan, 1988; Skelton, 1994;

Stanley, 1988; Wilde and Berry, 1984; Fortey, 1989; Wang et al., 1993a,b; Yan et al., 2012; Zhang et al., 2009; Buggisch et al., 2010; Harper et al., 2013).

The LOME occurs in two discrete pulses over the course of approximately 1.5 My: the first at the beginning of the Hirnantian and the second near the end Hirnantian (Brenchley, 1994; Sheehan, 2001; Finnegan et al., 2011). The first pulse was believed to be related to shallow marine habitat loss due to glacio-eustatic sea-level fall as a result of short-lived but intense glaciation on the southern continent of Gondwana coupled with an associated cooling of the oceans (Berry and Wilde, 1978; Brenchley et al., 1994; Finnegan et al, 2012). Recent evidence, however, shows that the initiation of the first pulse starts during a period of melting, not cooling (Ghienne et al., 2014).

The first pulse primarily affects animals occupying shallow and very deep water environments; mid-water organisms are less impacted. Planktonic organisms, particularly graptolites and nektonic animals, were especially hard hit (Rasmussen and Harper, 2011). The second extinction pulse killed off many of the survivors of the first with the conodonts being greatly affected. However, neither pulse appears to have been particularly destructive to ecosystems considering the rapidity with which taxa rebounded with little or no changes to community structures (Droser et al., 2000; McGhee et al., 2004). The second extinction pulse has a distinctly different selective signature than the first (Finnegan et al., 2012), suggesting that it is not caused by the same mechanism. Lithologic and geochemical evidence suggests widespread marine anoxia/euxinia is associated with the second faunal turnover (Sheehan, 2001a, Brenchley et al., 2003; Rasmussen and Harper, 2011b; Harper et al., 2013); however, it occurs during a period of intensifying glaciation in contrast to most other Phanerozoic anoxic events.

2.5. Anticosti Island

Well-dated and complete marine successions of the Upper Ordovician extinction interval are limited because of its coincidence with glacio-eustatic lowstand conditions. Platform carbonates on Anticosti Island, Canada are well studied and represent one of the most complete successions, including the paleontology, biostratigraphy, sequence stratigraphy, and stable isotope stratigraphy (Desrochers et al., 2010; Finnegan et al. 2012; Achab et al. 2013; Copper and Jin, 2014; Ghienne et al., 2014; Mauviel and Desrochers 2016). The 100m thick Upper Ordovician through Lower Silurian succession was unaffected by Ordovician Taconic deformation, was buried less than 1 km implying minimal burial diagenesis, and has not been dolomitized (Petryk, 1981; Sami and Desrochers, 1992; Cocks and Torsvik, 2004; Long, 2007).

The mid Katian, Hirnantian, through lower Rhuddanian studied interval is composed of offshore (dysoxic), lower shoreface (dysoxic to oxic), through shoreface and patch-reef (oxic) facies (Desrochers et al., 2010). The facies are arranged into 5 transgressive-regressive depositional sequences (2-17m thickness) and internal meter-scale cycles/parasequences (Fig. 2; Long, 1993; Desrochers et al., 2010, Ghienne et al., 2014). These sequences have been biostratigraphically correlated to shallow marine siliciclastic and glaciogenic deposits in Anti-Atlas, Africa documenting glacio-eustasy as the primary driver for the <0.4 My scale sequences and directly links the timing of these eustatic changes with associated faunal diversity changes and carbon isotope excursions derived from Anticosti Island (Ghienne et al., 2014). The globally recognized Hirnantian positive carbon isotope excursion (HICE) is well documented on Anticosti Island where it is particularly thick due to the relatively high sedimentation rates and spans the entire Hirnantian interval

(Fig. 2). Background values of <1 ‰ increase to ~2 ‰ in the early Hirnantian, drift back to near background values in the mid Hirnantian, abruptly shift to ~4 ‰ in the latest Hirnantian, then abruptly return to background values in the early Rhuddanian. Peak C-isotopic values occur just after maximum glacio-eustatic lowstand conditions and during the initial deglaciation (Ghienne et al., 2014).

2.6. Late Ordovician marine anoxia

The late Katian appears to be a time of relatively widespread anoxia which is reflected in sediments deposited on Laurentia, Baltica, Siberia, Avalonia and China (Fig 6) with an apparent concentration in the paleotropics (Melchin et al., 2013), though some paleotropics locales appear to have been oxic. Anoxia appears to abate during the mid-Hirnantian with only sporadic evidence for anoxic depositional conditions and no apparent depth dependency. Widespread anoxia returns during the Early Rhuddanian with sedimentological evidence for deposition under anoxic/dysoxic conditions present on all continents (Melchin et al., 2013). There does appear to be a discordance between the sedimentological evidence for anoxic/euxinic conditions globally and the results of this study but it is important to consider that such evidence represents, at best, an incomplete record and that significant selection biases and correlation errors may limit the temporal resolution of such studies.

Changes in Late Ordovician marine redox conditions are derived from sedimentological, biochemical and geochemical evidence. Sedimentological evidence for Late Ordovician anoxia includes the widespread occurrence of organic-rich, pyrite-bearing marine deposits lacking evidence of bioturbation (Armstrong and Coe, 1997; Finney et al., 1999) and from pyrite

size/abundance trends (Hammarlund et al., 2012). Biochemical evidence consists of lipid biomarkers (Rohrssen et al., 2013). Geochemical evidence for Late Ordovician redox trends comes from variations in redox sensitive metals, pyrite sulfur isotopes, reactive Fe abundances, and $\delta^{13}C$ trends (Goodfellow and Jonasson, 1984; Wang et al., 1993 a, b; Brenchley et al., 1994; Finney et al., 1999; Bergstrom et al., 2006; Kump et al., 1999; Zhang et al., 2009; Yan et al., 2012). Survey studies show convincing evidence for global anoxic conditions during the early Rhuddanian (Fig. S3). Except for $\delta^{13}C$ trends, these sedimentologic and geochemical proxies evaluate local bottom water or porewater redox conditions and require analysis from multiple coeval successions to verify the global nature of the signal. In contrast, U isotopes from marine carbonates provide a potential global redox proxy.

2.7. Uranium isotope systematics

Uranium is the heaviest naturally occurring element and occurs naturally in three isotopes: ^{238}U (99.3%), ^{235}U (0.7%) and ^{234}U (0.005%). Uranium in the modern ocean occurs in two dominant oxidation states: the insoluble U^{4+} and the highly soluble U^{6+} (Djogic, 1986). In oxidizing marine environments, U is mostly present in the U^{6+} form as the uranyl ion UO_2^{+2}. In this form U is highly mobile, forming soluble complexes with both carbonates and phosphates. In reducing marine environments, U occurs as U^{4+}, is mostly insoluble (Ivanovich and Harmon, 1992), and displays non-conservative behavior in that it is removed from seawater and sequestered into sediments formed under such conditions (Klinkhammer and Palmer, 1991; Dunk et al., 2002).

The primary input of U to the modern ocean is riverine with a small and poorly constrained contribution from eolian and groundwater/estuary sources (Dahl et al., 2014). There are three major sinks for U in the modern oceans: biogenic carbonates, anoxic sediments (<10-6 mol H_2S L^{-1}, <10-5 mol O_2 L^{-1}) and suboxic (10-5 to 10-4 mol O_2 L^{-1}) sediments (Morford and Emerson, 1999; Dunk et al., 2002; Henderson and Anderson, 2003; Noordmann et al., 2015). Modern seawater has a $\delta^{238}U$ (Equation 1) value of ~ -0.392 ±0.005 ‰ relative to CRM-112a (Stirling et al., 2007; Weyer et al., 2008; Romaniello et al., 2013; Dahl et al., 2014; Tissot and Dauphas, 2015) whereas modern riverine input has a $\delta^{238}U$ of ~ -0.24 ±0.05 ‰ relative to CRM-112a (Stirling et al., 2007; Dahl et al., 2014; Tissot and Dauphas, 2015) (Fig. S4).

$$\delta^{238} = \frac{\left(\frac{U^{238}}{U^{235}}\right)_{sample} - \left(\frac{U^{238}}{U^{235}}\right)_{std}}{\left(\frac{U^{238}}{U^{235}}\right)_{std}} \times 1000$$

Equation 1. $\delta^{238}U$ values are reported using standard delta notation.

The small difference in mass (less than 1%) between ^{238}U and ^{235}U severely limits mass fractionation in uranium. Mass fractionation among U isotopes is less than 1/20th of that found in iron, for example (Stirling et al., 2007). The ratio of ^{238}U to ^{235}U has therefore been largely treated as an invariant. However, elements with large atomic numbers can undergo significant equilibrium isotopic fractionation due to their nuclear volume. This effect is called the nuclear field shift and is a result of the overlapping of nuclear and electron wave functions (Bigeleisen, 1996a, b; Schauble, 2007). As a result of this effect, the lighter isotope of uranium is preferred in the oxidized species while the heavier is preferred in the reduced state. This effect is dominated by nuclear volume with mass fractionation playing a minor role. When U^{6+} undergoes reduction to U^{4+}, ^{238}U preferentially participates in the reduction reaction with respect to ^{235}U. This leads to an enrichment in ^{238}U in

sediments compared to ^{235}U when U is precipitated under anoxic or suboxic conditions (Stirling et al., 2007; Weyer et al., 2008).

The removal of U from seawater under suboxic or anoxic conditions occurs mostly in sediment porewaters rather than directly from the water column, with most of the U delivered in the form of dissolved U^{6+}. Modern sediments deposited under anoxic conditions have an average Δ238/235 (anoxic-SW) of ~ 0.6 ‰ whereas those deposited under suboxic conditions have a Δ238/235 (subanoxic-SW) of ~ 0.2 ‰ (Dunk et al., 2002; Weyer et al., 2008; Dahl et al., 2014; Tissot and Dauphas, 2015). During deposition under oxic conditions, U may be removed via adsorption during the formation of Mn nodules; this process produces a fractionation of approximately 0.2 ‰ (Stirling et al., 2007; Weyer et al., 2008; Tissot and Dauphas, 2015). It is also possible that banded iron formations (BIF) may have played an important role in ancient anoxic oceans. While the formation of Mn nodules or BIFs play a relatively minor role in the modern oceans, their role in the Ordovician oceans is uncertain (Asael et al., 2013).

Uranium can also be incorporated into carbonates by absorption or adsorption; neither process produces a significant isotopic fractionation (Fig. S5; Stirling et al., 2007; Weyer et al., 2008; Romaniello et al., 2013). This fact allows for the preservation of a seawater $\delta^{238}U$ signal in marine carbonates. Given that the sequestration of uranium in sediments via reductive scavenging from U^{6+} to U^{4+} is the principal means of removing U from seawater (Klinkhammer and Palmer, 1991; Morford and Emerson, 1999; Dunk et al., 2002; Henderson and Anderson, 2003), coupled with its relatively long residence time (<400 ky) with respect to ocean mixing times (< 1 ky), the global extent of anoxic/suboxic deposition will be reflected in the $\delta^{238}U$ values of seawater (Ku et al., 1977; Chen et al., 1986). This allows for the

use of $\delta^{238}U$ recorded in marine carbonates to serve as a proxy for global redox conditions.

The Th/U ratio preserved in marine carbonates can also serve as a global paleoredox proxy because Th has only one oxidation state (Th^{4+}). An increase in the area of anoxic/euxinic sediment deposition would draw down marine U concentrations while not affecting Th. (Wignall and Myers, 1988; Brennecka et al., 2011). Additionally, since the source of both U and Th in the oceans is continental, the addition of either element via increased runoff or weathering would not affect the Th/U ratio (Wignall and Myers, 1988; Jones and Manning, 1994).

3. Materials and methods

Samples were collected at the La Framboise section on western Anticosti Island from offshore through upper shoreface and patch-reef facies (Desrochers et al., 2010). Samples were collected every 10-20 meters from the upper Katian to upper Hirnantian, then every 1-2 meters across the upper Hirnantian through lower Rhuddanian (Fig. 2). Powdered samples for isotopic, elemental concentrations, and total organic carbon (TOC) analysis were prepared from clean, unweathered hand sample chips with no veins for fractures. U-isotopic analyses were performed at the Radiogenic Isotope Laboratory at the University of New Mexico. All lab work was performed in Teflon beakers cleaned by boiling in Aqua Regia followed by boiling in $HN0_3$ then in 19 MΩ H_2O. For U-isotopic analysis, approximately 150-200 mg of powder was dissolved in 1N acetic acid for several hours until no reaction was observed; acid insoluble residues were separated from the solute by centrifuging, followed by the addition of a calibrated IRMM-1 spike with known $^{236}U/^{233}U$ and ^{229}Th values, fluxed, dried down, then dissolved in 7N HNO_3 for column separation. U and Th were collected using 0.5 mL anion exchange

resin columns and the separates were dried and dissolved in 3% HNO_3 for analysis. Since all of the samples were not processed at the same time, samples were duplicated between batches to insure run to run repeatability and to insure against contamination during preparation and analysis (Fig. S12). In addition, a single sample horizon (LF-13) containing a mostly complete rugose coral, the septum and fossula were drilled out (excluding as much of the matrix material as possible), was powdered and analyzed (Fig. S12).

For TOC, approximately 5 mg of powder was dissolved using HCl in 40mg silver capsules. The cup and sample were then dried down and TOC measurements were performed at the UNM Center for Stable Isotopes.

4. Results

Measured $\delta^{238}U$ values range from 0.44 ‰ to -0.83 ‰ relative to CRM-112a (Fig. 2, Table S1). Late Katian through late Hirnantian values average ~-0.22 ‰ with a single mid Hirnantian value of -0.83 ‰. In the late Hirnantian, there is an abrupt negative shift to values averaging -0.45 ‰, followed by an abrupt positive shift to values averaging 0.28 ‰ in the earliest Silurian (Rhuddanian). Th/U values average ~0.8 ‰ during the late Katian to late Hirnantian and shift to an average of ~2.2 ‰ in the late Hirnantian before returning to an average of ~1 ‰.

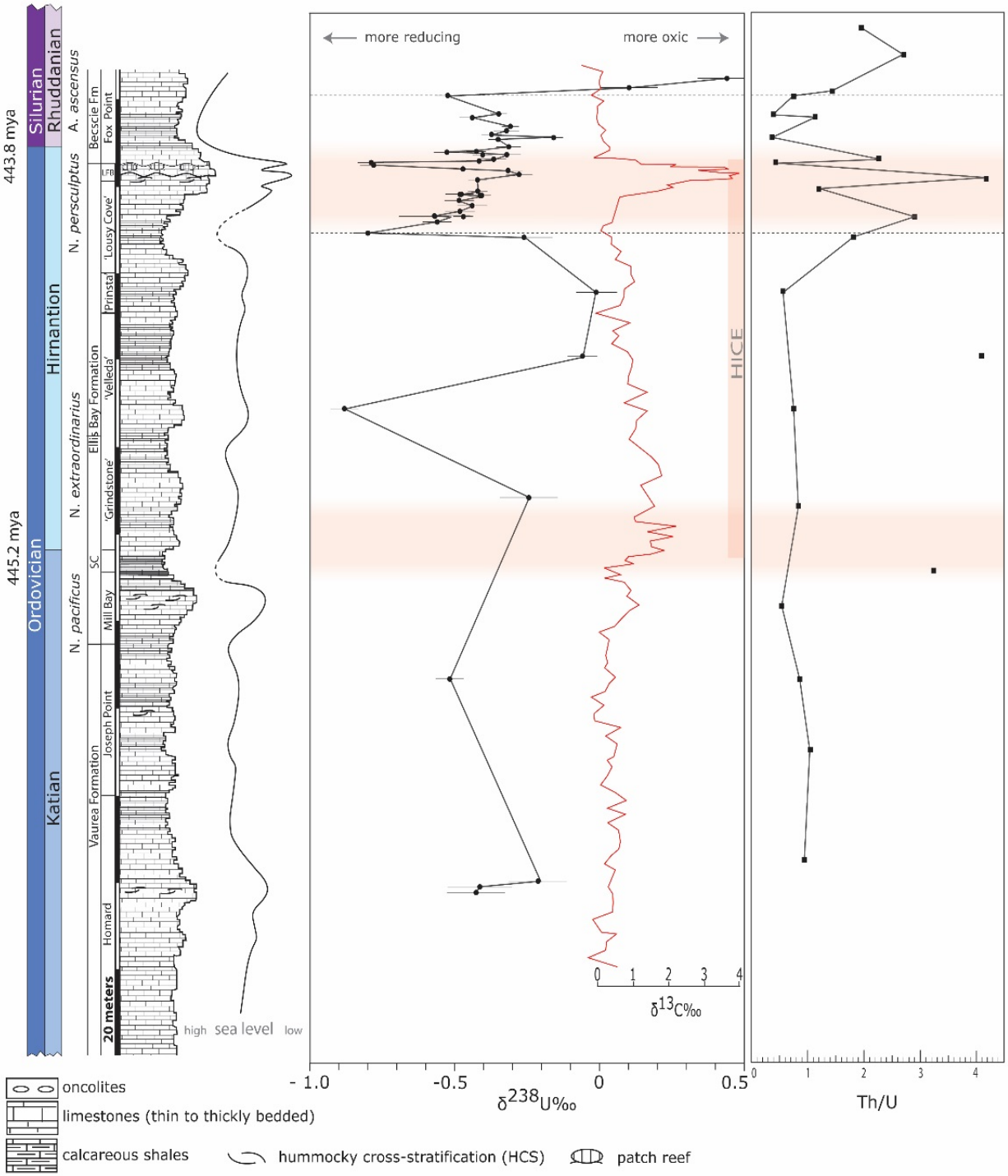

Fig. 2. Integrated sedimentological and geochemical stratigraphy for Anticosti Island, Canada. Sea level curve, stratigraphy and d^{13}C curve adapted from Wickson, 2010 and Ghienne et al., 2014. Colored bands denote the two extinction pulses of the LOME. Horizontal dotted lines outline the onset and end of the abrupt δ^{238}U excursion or HOAE. For a larger version of this diagram refer to the supplemental materials.

5. Discussion

5.1. Evidence for primary signal

To verify that bulk carbonate $\delta^{238}U$ values represent a global redox proxy, we evaluate whether the measured values record local depositional conditions (local bottom water anoxia or local detrital influx of U) or have been altered by diagenesis (carbonate cements precipitated from anoxic or meteoric porewaters).

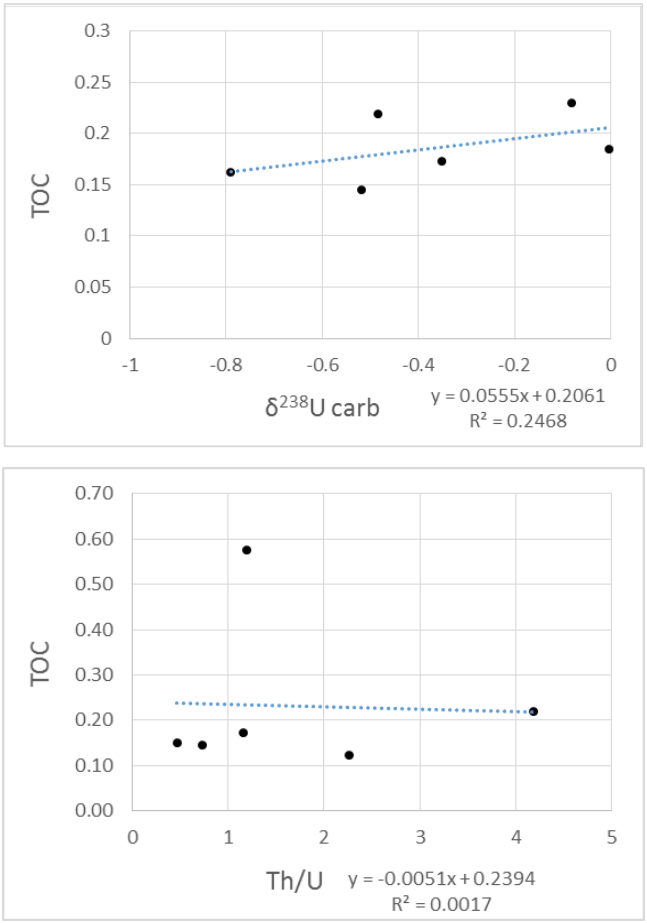

Fig. 3. TOC versus $\delta^{238}U$ (top) and TOC versus Th/U (bottom) cross plots for the late Hirnantian (162m-126m).

The main line of evidence against local anoxic bottom waters controlling $\delta^{238}U$ values is that the onset of the abrupt late Hirnantian negative $\delta^{238}U$ shift occurs in a monotonous succession of dysoxic offshore lime mudstones and the low $\delta^{238}U$ values continue despite the change into overlying oxic lower shoreface, upper shoreface, patch reef, and dysoxic offshore facies (Fig. 3). In other words, $\delta^{238}U$ values are not facies-controlled and remain negative despite the fact that the local facies change from dysoxic to oxic depositional conditions. Of particular importance is that the negative isotopic trends occur within photic zone facies, which, due to wave mixing,

were presumably in equilibrium with atmospheric oxygen levels yet these deposits still record low $\delta^{238}U$ values.

High sediment TOC concentrations could indicate local bottom waters had low dissolved oxygen concentrations or could lead to rapid porewater oxygen depletion resulting in precipitation of early marine cements with elevated $\delta^{238}U$ values (Romaniello et al., 2013). Measured TOC concentrations are low, averaging ~0.2%, and there is little correlation between $\delta^{238}U$ versus TOC values and TOC versus Th/U values (Fig. 3), suggesting that sediment TOC concentrations did not influence measured $\delta^{238}U$ or Th/U trends.

Marine limestones, even those deposited under oxic conditions, likely record $\delta^{238}U$ values from primary carbonate precipitates and early through late diagenetic cements (Fig. S6). Early marine cements precipitated while porewaters are still in communication with bottom waters should reflect overlying seawater $\delta^{238}U$ values. The measured bulk carbonate $\delta^{238}U$ values could also contain a signature reflecting late burial cements which precipitated from anoxic porewaters; these cements would be enriched with respect to original seawater values and shift the bulk limestone to higher isotopic values (Barnes and Cochran, 1993; Morford et al., 2005; McManus et al., 2006; Morford et al., 2009, Romaniello, et al. 2013). Isotopic values from bulk limestones in this study should yield $\delta^{238}U$ values that are equal to or larger than that of the Late Ordovician oceans (Fig. S9) (Romaniello et al., 2013; Andersen et al., 2014), having been overprinted by cements precipitated in potentially anoxic porewaters or from meteoric waters (which have higher riverine $\delta^{238}U$ values) affecting the deposits during sea-level lowstands. The magnitude and direction of this shift conforms to the measured shift between a rugose coral (primary precipitant) and bulk-rock $\delta^{238}U$ values (Fig. S12) performed in this study. A necessary underlying assumption of this study is

that any contributions from late burial cements is uniform throughout the studied section; therefore, observed isotopic trends reflect original Late Ordovician seawater variabilities but absolute values may have shifted.

The potential for detrital U input affecting the measured $\delta^{238}U$ seems very unlikely as typical riverine or continental $\delta^{238}U$ values are higher than seawater (Stirling et al., 2005, 2007; Weyer et al., 2008; Telus et al., 2012, Tissot and Dauphas, 2015), so any input from those sources would shift typical marine carbonate values higher rather than lower. This also applies to the effects of potential meteoric diagenesis during subaerial exposure related to late Hirnantian glacial lowstand conditions because any such cements would shift bulk marine carbonates to higher rather than lower values. Instead, measured $\delta^{238}U$ values directly above and below the main late Hirnantian glacial lowstand (subaerially exposed at times) unconformity record some of the lowest values in the section, implying they were not affected by meteoric U input.

The combined facies and geochemical evidence suggest that the observed $\delta^{238}U$ trends do not reflect local depositional conditions, arguing instead that they record global Late Ordovician seawater redox trends. We acknowledge that the effects of early through late burial cementation likely enriched all original $\delta^{238}U$ values, but the above arguments suggest that the relative trends reflect original seawater variabilities.

5.2. Correction for contribution from anoxic porewater derived cements

Despite arguments that the measured trends represent original Late Ordovician trends, we recognize that average measured values (~-0.25 ‰) are higher than modern $\delta^{238}U$ seawater values (-0.392 ±0.005 ‰ ; Romaniello

et al., 2013; Tissot and Dauphas, 2015). Late Ordovician seawaters that are more oxic than modern seawater is not reasonable because 1) Ordovician atmospheric oxygen levels were lower (Fig. S7; Bergman et al., 2004; Berner, 2009; Dahl et al., 2010) and presumably seawater-dissolved oxygen concentrations were also lower, 2) previous U-isotope studies from time periods when pO_2 was similar to the modern value record $\delta^{238}U$ seawater values that are similar to modern seawater (Montoyo-Pino et al., 2010; Brennecka et al., 2011; Lau et al., 2016), while $\delta^{238}U$ values from time periods with lower pO_2 show more positive values (Dahl et al., 2014). It has also been shown that $\delta^{238}U$ values of shallow-buried modern Bahamian carbonates are enriched in $\delta^{238}U$ due to anoxic porewater diagenesis (Romaniello et al., 2013). These combined results indicate that to use absolute Ordovician values in any quantitative modeling, a positive 'diagenesis correction' factor of about 0.2-0.4 ‰ needs to be applied (Romaniello et al., 2013).

6. Late Hirnantian anoxia

6.1. The Hirnantian OAE

We refer to the late Hirnantian negative $\delta^{238}U$ excursion as the Hirnantian ocean anoxic event or HOAE. To estimate its duration and timing of onset and end, we calculate Hirnantian average sedimentation rates at Anticosti Island. The current estimate on the Hirnantian stage duration is ~1.4 ± 0.2 My (Cohen, et al., 2013). At Anticosti Island, the studied Hirnantian interval is ~92 m thick yielding an average sedimentation rate of ~6.5 cm/ky. Applying this rate to the HOAE thickness interval (~30 meters) suggests an HOAE duration of ~450 ky with the start and end of the excursion occurring within less than 20 ky. Post-HOAE values are significantly higher than pre-excursion values suggesting that the earliest Silurian oceans were better ventilated than before the excursion, at least temporarily, and that

during the HOAE there appears to be an overall increase in $\delta^{238}U$ values (superimposed upon higher frequency variability) that may foreshadow the abrupt return to more oxic seawaters.

The onset of the HOAE is coincident with the start of the second LOME pulse but ends approximately 200 ky after the extinction pulse ends. This is consistent with the hypothesis that widespread ocean anoxia was responsible for the second extinction pulse. Lack of precision with regard to the duration of the extinction pulse may negate any difference in duration between it and the HOAE.

The HOAE onset coincides with high glacio-eustatic sea levels that occurred in the deglacial interval just before peak late Hirnantian glacial conditions (Fig. 2). These results differ from previous studies that interpret widespread latest Hirnantian-early Rhuddanian anoxia as occurring after the peak late Hirnantian glaciation (Page et al., 2007; Melchin et al., 2013). This timing difference in HOAE onset is likely due to complications related to biostratigraphic correlations between stratigraphic sections recording sea-level history (proxy for glacial history) and sections with sedimentary evidence for anoxic conditions. The fact that the sequence stratigraphy, biostratigraphy, faunal diversity records, and $\delta^{238}U$ redox signal all come from the Anticosti Island section alleviates any potential timing mismatches. The results of this study indicate a return to oxic conditions, at least temporarily, in the early Rhuddanian; this is in contradiction to extensive sedimentological evidence which suggests that anoxia persisted through the Rhuddanian (Melchin et al., 2013). It is possible that the abrupt return to more oxic conditions is only a transient event and if additional samples were available from the remaining Rhuddanian, we would observe a return to anoxic conditions in keeping with that observed in the sedimentologic record by Melchin et al. (2013); (Fig.S3).

Widespread marine anoxia during sea-level rise and highstand has been interpreted in many previous studies and in the Late Ordovician in particular is attributed to increased continental runoff (due to climatic warming) and meltwater discharge (deglaciation) which combine to increase nutrient flux and strengthen the pycnocline. Higher primary productivity across the wider flooded continental margins leads to increased oxygen demand and a resultant oxygen minimum zone (OMZ) expansion (Page et al., 2007; Melchin et al., 2013). This study, however, documents that the HOAE initiated during peak deglacial conditions and glacio-eustatic highstand and persisted through the peak Hirnantian glacial interval (sea-level lowstand) and ensuing deglaciation (rising sea level).

6.2. The HOAE and its relationship to the HICE

The HOAE is roughly coincident with the large positive $\delta^{13}C$ shift at the HICE termination (Fig. 2); however, the high-resolution record afforded by the Anticosti Island section permits detailed comparisons between the timing of the HOAE and HICE that is not possible at other locations. The HOAE onset begins approximately 120 ky before the large positive $\delta^{13}C$ shift and continues for ~250 ky after its end. This mismatch in timing suggests that the processes influencing global carbon burial rates are temporally distinct from those influencing global marine anoxia. Decoupling between $\delta^{238}U$ or other anoxia proxies and $\delta^{13}C$ trends is also reported by Dahl et al. (2014), Lau et al. (2016) and Elrick et al. (submitted). Weathering of marine carbonates exposed during regressions has been proposed (Page et al., 2007) as a mechanism for decoupling of $\delta^{13}C$ values and anoxia. This is a possible cause for the offset between the onset of anoxia and the large positive $\delta^{13}C$ shift present in the late Hirnantian as it occurs during such a regression.

6.3. Comparison to other OAEs

The HOAE is similar in duration and abrupt onset/end to previously reported Paleozoic and Mesozoic OAEs (e.g., Silurian: Munnecke et al., 2003; Cramer and Saltzman, 2005; Cretaceous: Leckie et al., 2002; Jenkyns, 2010); (Fig. S10). Despite the temporal similarities, the HOAE differs from other well-documented OAEs in that it occurs during peak icehouse conditions rather than during a greenhouse climate and only a portion of it is associated with a positive $\delta^{13}C$ shift. These results require some mechanism(s) unrelated to greenhouse climates and low seawater oxygen solubility to drive HOAE development.

7. HOAE Model

To estimate the increase in area of anoxic deposition required to generate the observed $\delta^{238}U$ isotopic shift, we use a simple box model described in the Supplementary Materials and Figures S8 and S9. The model adjusts the main U sinks (oxic, dysoxic, and anoxic/euxinic deposition and altered basalts; Dahl et al., 2014) to match riverine input with an average Late Ordovician ocean $\delta^{238}U$ value of -0.45 ‰ plus a -0.25 ‰ diagenetic correction factor which was chosen as a conservative number within the suggested range of -0.2 ‰ – -0.4 ‰ (Romaniello et al., 2013). We assume a constant riverine input to the oceans with an average value of −0.24‰; constant respective fractionation coefficients for the various U sinks and a constant flux per unit area of U into anoxic sediments. Using this simple model to generate the observed -0.35 ‰ HOAE shift, the area of anoxic deposition would have increased by ~7 times. This increase is similar to previous studies for the Cretaceous OAE-2, the late Permian mass extinction, and the Late Cambrian anoxia event (SPICE) (Fig. S10; Montoya-Pino et al., 2010;

Brennecka et al., 2011; Dahl et al., 2014). For comparison, the total area of modern anoxic seafloor deposition is less than 0.3% (Tissot and Dauphas, 2015), so increasing this amount by 7 times equates to ~2% of the Ordovician seafloor accumulating anoxic sediments. It is also worth noting that it is not possible to produce the observed $\delta^{238}U$ shift by increases in dysoxic sediment sinks or fractionation by altered basalts alone owing to their lower fractionation coefficients.

Given that there are three basic ways to explain widespread marine anoxia: lowering of atmospheric O_2, significantly reducing or halting deep sea ventilation (ocean stagnation) and an increase in primary productivity, it is necessary to interpret the results of this study in terms of these potential causes. First, let us consider low atmospheric O_2 as a driver for the HOAE. While it is true that atmospheric O_2 was considerably lower during the late Hirnantian, it was at such levels or lower for the majority of the Hirnantian. It has also been as low or lower during many periods of Earth's history which did not feature widespread marine anoxia (Fig. S7). For example, the entire Jurassic and first half of the Cretaceous featured similar levels of atmospheric O_2 (Berner, 1994; 2009). Secondly, we will consider the possibility of ocean stagnation causing the occurrence of widespread anoxic conditions and an accompanying increase in deposition under such conditions. Many consider the strong chemical stratification required to produce such global anoxia to require sluggish oceanic circulation as in the Black Sea model (Arthur & Sageman, 1994). Given recent computer modeling, it appears that ocean stagnation is not sufficient to cause widespread marine anoxia (Meyer and Hotinski et al., 2001; Kump, 2008). It is also very unlikely given the stability of such a stagnant ocean that even if such anoxia was produced that it could persist for the length of time suggested for the HOAE (Worthington, 1968; Thual and McWilliams, 1992; Saravanan and McWilliams, 1995). Given the

unlikelihood of the aforementioned cause, increased primary productivity seems the most likely causative mechanism for the HOAE.

We interpret that the HOAE was driven primarily by late Hirnantian cooling (Trotter et al., 2008) and the resultant steeper pole-to-equator thermal gradient. The steeper thermal gradient led to increased atmospheric and oceanic circulation rates, creating more vigorous coastal upwelling and thermohaline circulation and increased bottom water nutrient delivery to the surface water photic zone (Fig. 5). The increase in primary productivity resulted in a greater demand for dissolved oxygen and an expansion of the OMZ. The intersection of the expanded OMZ with the seafloor increased the area of

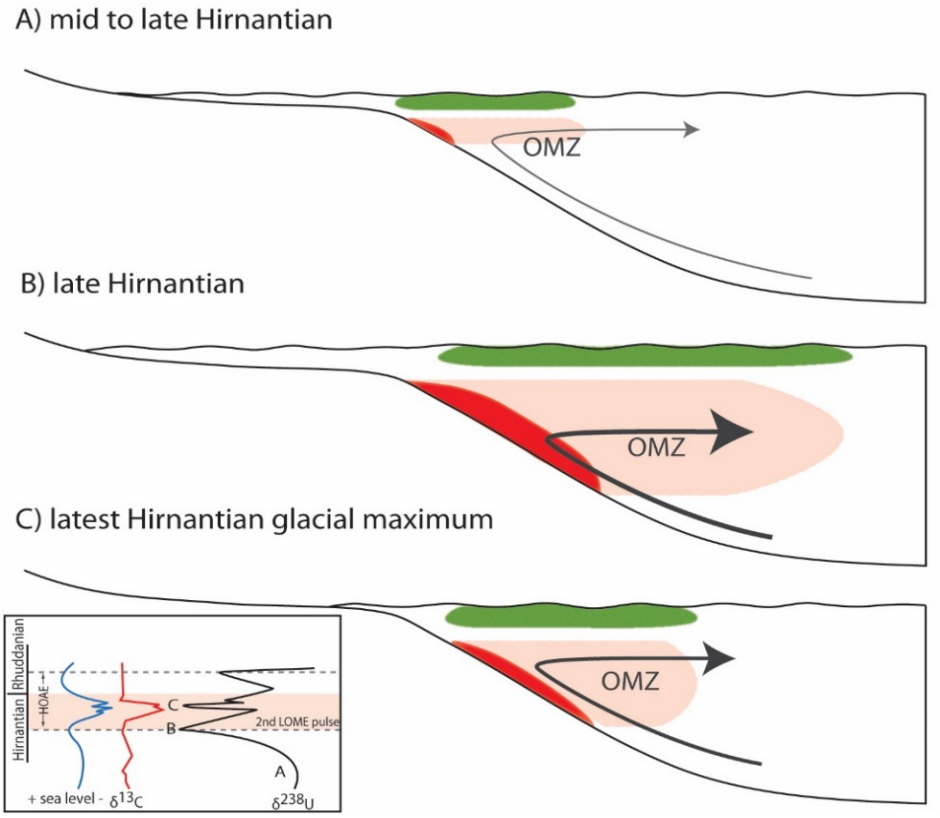

Fig. 5. Schematic model showing changes in anoxic deposition, ocean circulation, and upwelling. A) Mid to late Hirnantian prior to the onset of main glaciation and HOAE, weaker thermohaline circulation/upwelling and partial flooding of continental shelf with minor anoxic sediment deposition. B) Late Hirnantian, during early onset of HOAE and glaciation with increasingly vigorous thermohaline circulation/upwelling and expansion of OMZ. C) Glacial maximum, vigorous thermohaline circulation/upwelling, and continental-derived nutrient bypass. Note that the area of anoxic sediment deposition shifts seaward with sea-level fall. Inset shows idealized sea-level, carbon and U-isotope curves with letter indicating the respective time slice depicted.

anoxic sediment deposition and preferential $^{238}U^{4+}$ sequestration, leading to a negative $\delta^{238}U$ shift in global seawater values.

While we suggest that global cooling was primarily responsible for the HOAE, the rapidity of the onset (<20 ky) suggests that some threshold was reached to trigger abrupt anoxia onset. It is not clear what this threshold represents; it is possible that it is related to either the onset or vigor of thermohaline circulation or that perhaps it represents a change in global circulation mode, such as that proposed by Cramer and Saltzman (2005) to explain the Wenlock (Silurian) Carbon isotopic excursion (Fig. S11) and its associated anoxia. The <20 ky duration of the HOAE onset is significantly shorter than modern U residence time (<400 ky) and implies that the U concentration in global seawater must have been significantly lower than at present, either as the result of a large drawdown of U prior to the Late Ordovician or as a result of lower levels of riverine delivery to the ocean.

The HOAE, along with many other OAEs, lasted for ~450 ky. Persistently high primary productivity rates needed to generate the expanded OMZ requires continuous nutrient delivery to sustain production and resultant seawater oxygen consumption and it is not clear how such conditions were maintained without nutrient delivery from additional sources. Melchin et al. (2013) suggest that sustained high primary productivity and anoxia in the Late Ordovician might be possible because once anoxia initiates it can be maintained: 1) sediment-sequestered phosphorous is more mobile in reducing conditions and would be recycled back into the water column (Ingall et al., 1993; Van Cappellen and Ingall, 1994) and 2) initial Late Ordovician terrestrial plant colonization increased continental weathering rates and enhanced nutrient delivery. Another possibility is that during peak glacio-eustatic fall and lowstand, continental-derived nutrients, which normally would have been

utilized along more nearshore regions of the wide epeiric seas, would be available farther seaward because of shoreline regression to partially replenish or reinforce that available farther offshore due to enhanced thermohaline-induced upwelling (Fig. 2).

7.1. Contributing causes?

It would appear likely given that widespread marine anoxia is not associated with glaciation at any other time in Earth's history that there may well have been contributing factors leading to the HOAE. It is very possible that lower atmospheric O_2 during the Late Ordovician lowered the threshold for an increase in primary productivity to produce such widespread marine anoxia. It is also possible that Hirnantian paleogeography coupled with the changing sea-levels contributed to the presence of very efficient nutrient traps, allowing for a given increase in nutrient delivery to have a much greater chance of producing anoxic conditions around the world. Perhaps the HOAE actually represents the response of the world's oceans to a unique set of atmospheric and geographic conditions instead of a single cause.

8. Conclusions

1) $\delta^{238}U$ trends preserved in Upper Ordovician through lowermost Silurian marine carbonates on Anticosti Island, Canada reflect global seawater redox changes characterized by more oxic conditions in the late Katian through late Hirnantian; an abrupt -0.35‰ negative $\delta^{238}U$ shift to more reducing conditions in the latest Hirnantian through earliest Silurian (lasting ~450 ky), followed by an abrupt return to more oxic seawater in the early Silurian. Box modeling of the HOAE suggests a ~7x increase in area of anoxic sediment deposition to generate the observed negative shift.

2) Unlike previous Late Ordovician studies, this new global redox record is derived from the same location that documents one of the most detailed records of glacio-eustasy (proxy for glaciation history), faunal diversity changes (extinction pulses) and $\delta^{13}C$ changes and thus permits direct temporal comparisons among proxy records. These comparisons indicate that the HOAE: a) initiated during the glacio-eustatic highstand before the peak late Hirnantian glaciation, continued through maximum sea-level lowstand and the ensuring rise and implies that the location of anoxic sediment deposition occurred far offshore and was not affected by major regressions and transgressions, b) onset coincides with the second LOME pulse but continued for ~200 ky longer than the biologic recovery, indicating anoxia played a key role in the second LOME pulse but did not affect the recovery and c) started ~ 100 ky before and continued ~250 ky longer than the globally recognized positive HICE $\delta^{13}C$ excursion implying that the processes influencing the global $\delta^{13}C$ record were decoupled from those driving the HOAE. This timing demonstrates that if anoxia was a causative agent in the second LOME pulse then life must have adapted to its presence during the faunal recovery.

3) The HOAE duration and abrupt onset and end are similar to other previously reported Paleozoic and Mesozoic OAEs; however, the HOAE occurred during peak icehouse rather than greenhouse climates. We interpret that the anoxic event was driven primarily by global late Hirnantian cooling (perhaps in concert with lower atmospheric O_2 levels and/or the presence of very efficient nutrient traps), intensified thermohaline and upwelling circulation enhancing primary productivity and dissolved seawater oxygen demands, followed by OMZ expansion. The increase in seafloor area under anoxic conditions leads to increased sediment ^{238}U sequestration and lower seawater $\delta^{238}U$ values.

Supplemental materials

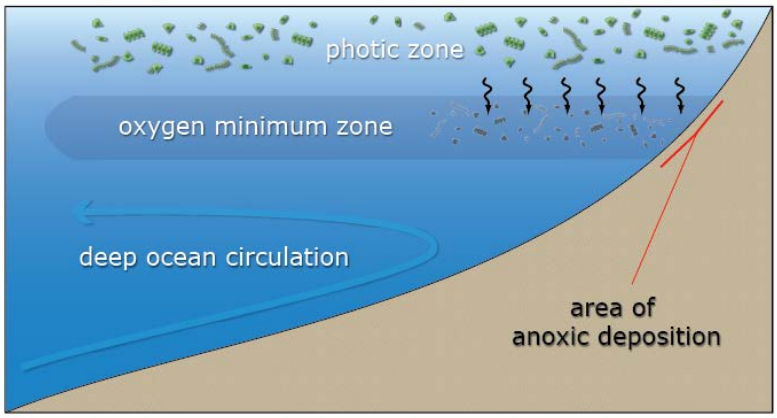

A

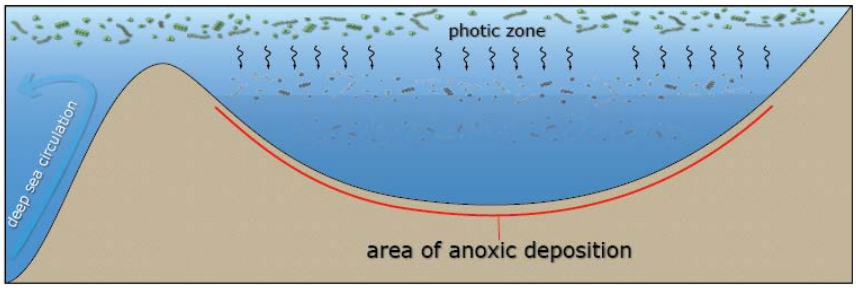

B

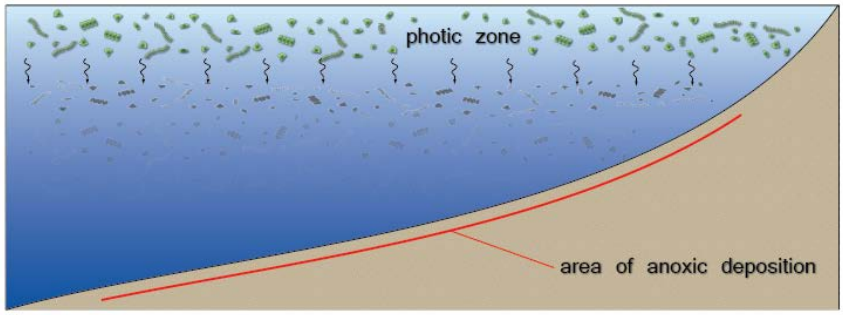

C

Supplemental Figure 1. A.) Bio-productivity in the photic-zone produces organic material that falls down through the water column undergoing decay; this decay consumes the available O_2 producing a zone of anoxic/euxinic conditions. Where this zone intersects the continent a zone of anoxic/euxinic deposition is formed. The oxygen minimum zone does not necessarily extend to the ocean bottom because of deep-water circulation. B.) Schematic of a restricted marine setting and its associated area of deposition under anoxic/exunic deposition. Such a system would be dependent on nutrients delivered from continental runoff. C.) Diagram showing the results of shutting down or greatly reducing deep ocean circulation as a mechanism for increasing the area of deposition occurring under anoxic/euxinic conditions.

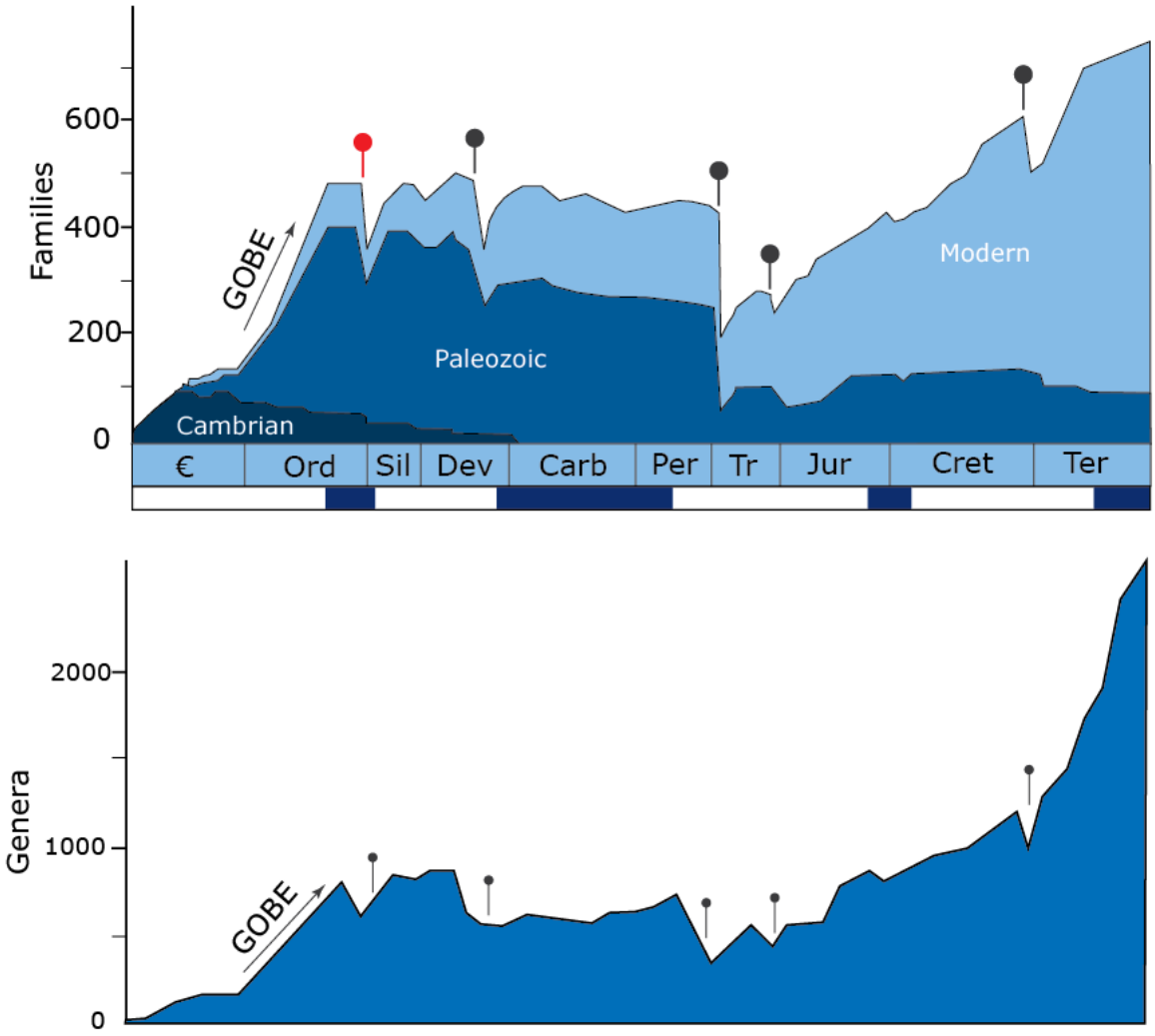

Supplemental Figure 2. (Top) Diversity curve of marine invertebrate families through the Phanerozoic (Sepkoski, 1996). (Bottom) The genera level curve (Alroy et al., 2008) derived from the paleobiological database. Black pins mark prominent extinction events. The Great Ordovician Biodiversification Event (GOBE) precedes the extinction event (LOME).

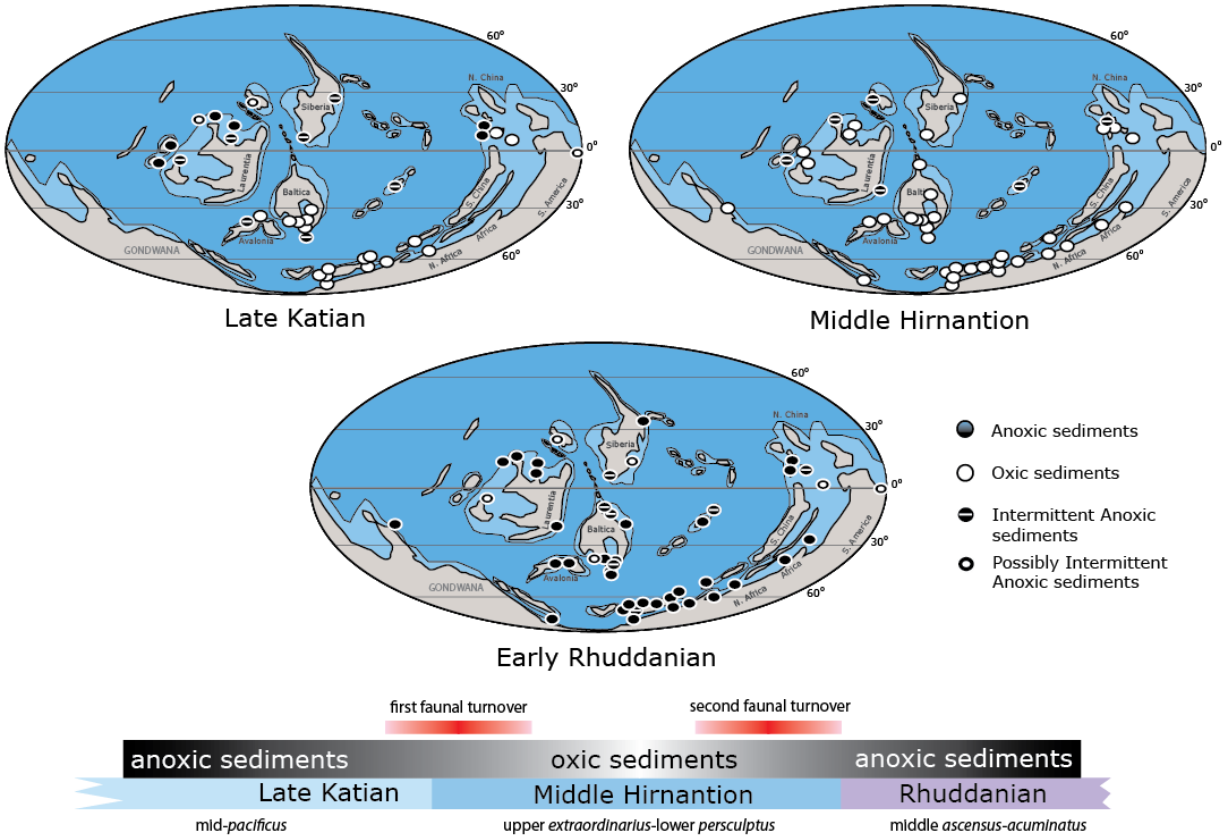

Supplemental Figure 3. Diagram showing Late Ordovician paleogeography and the various localities for which there is geochemical or sedimentological evidence for anoxic/euxinic conditions. Modified from Van Staal et al., (2010); Melchin et al., (2013); Pope and Steffen (2003) and paleogeographical reconstructions by Ronald Blakey.

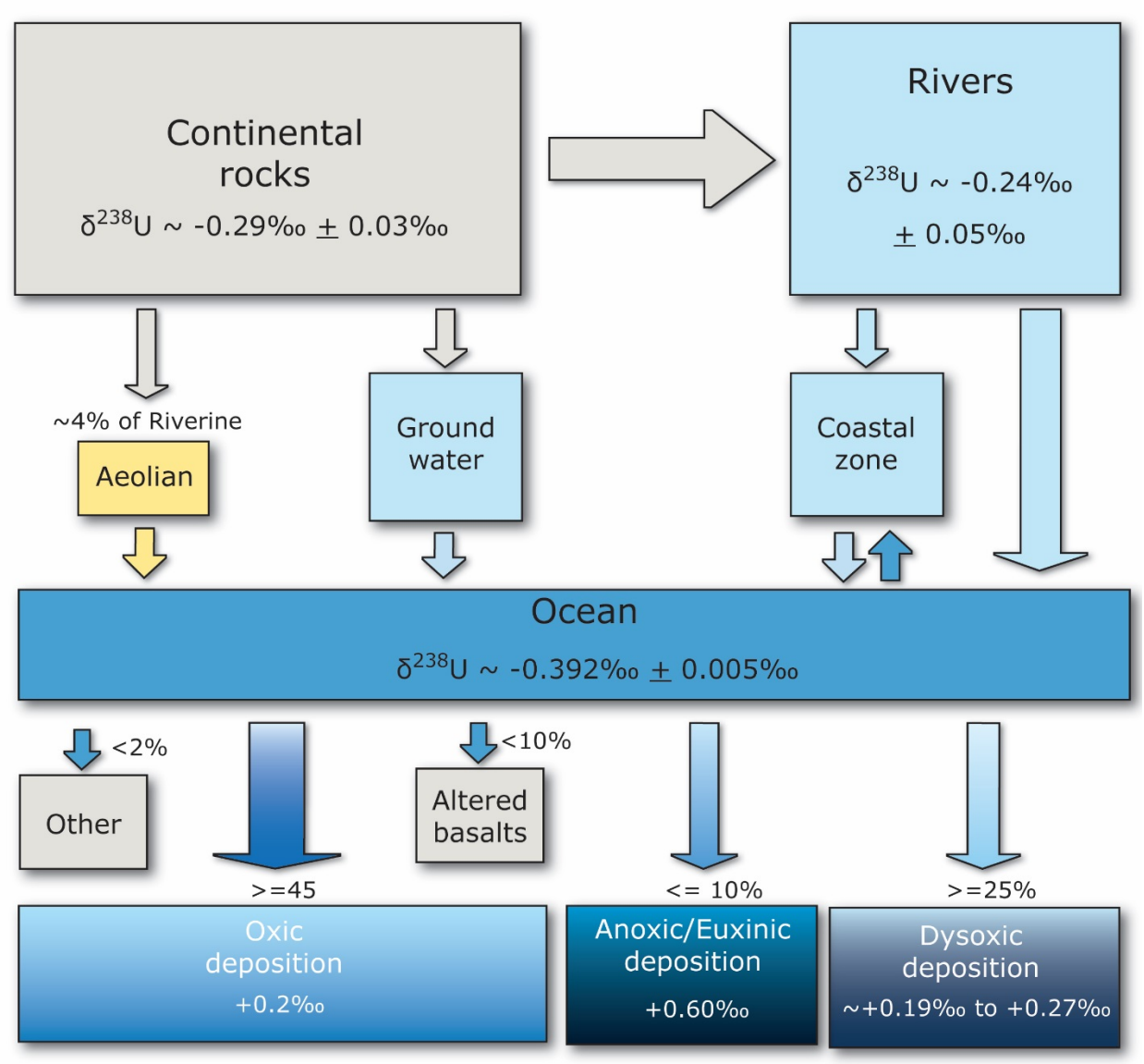

Supplemental Figure 4. Idealized box model for U in the ocean; values shown are for the modern ocean (modified from Weyer et al., 2008 and Dahl et al., 2014, Tissot and Dauphas, 2015). The percentage for each sink is approximate and modified from Dunk et al. (2002) and Tissot and Dauphas (2015).

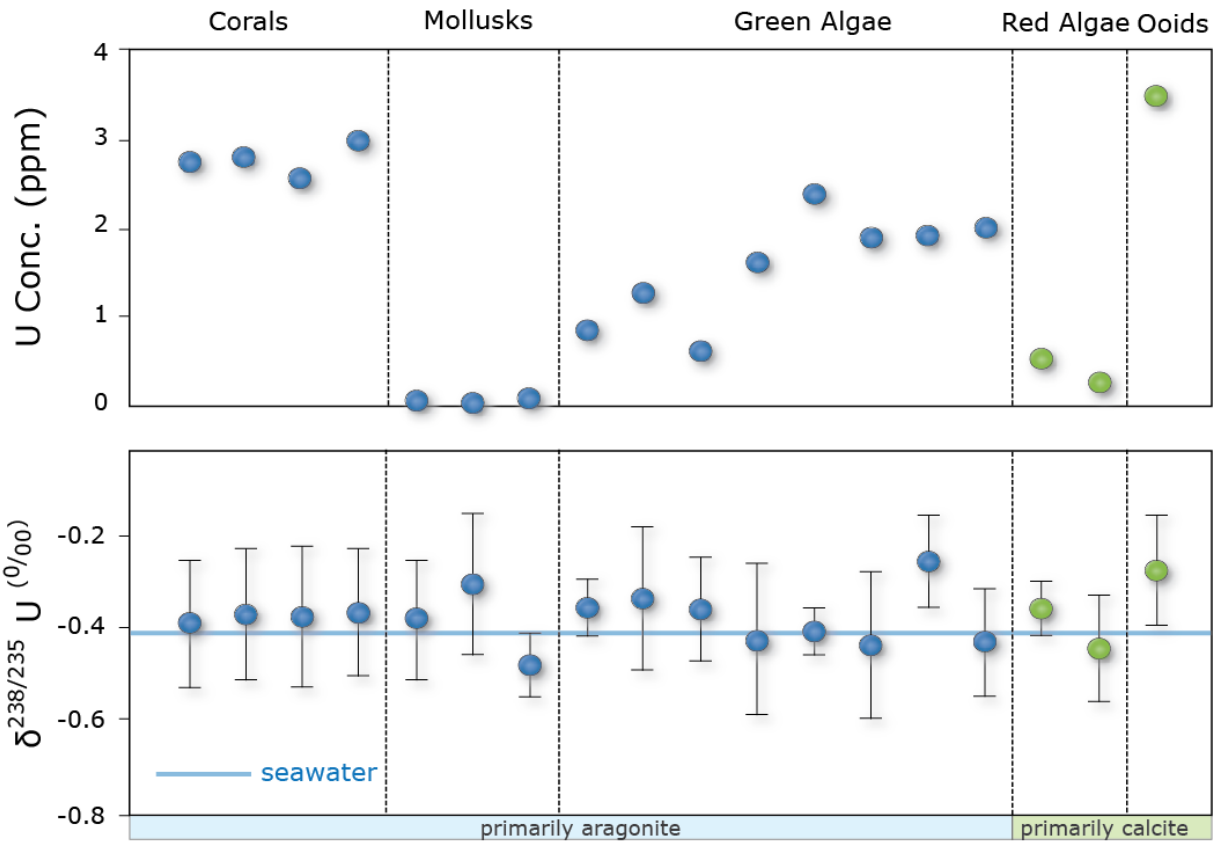

Supplemental Figure 5. U concentration (top) and $\delta^{238}U$ values (bottom) for various modern Bahamian primary precipitates compared to seawater values (modified from Romaniello et al., 2013).

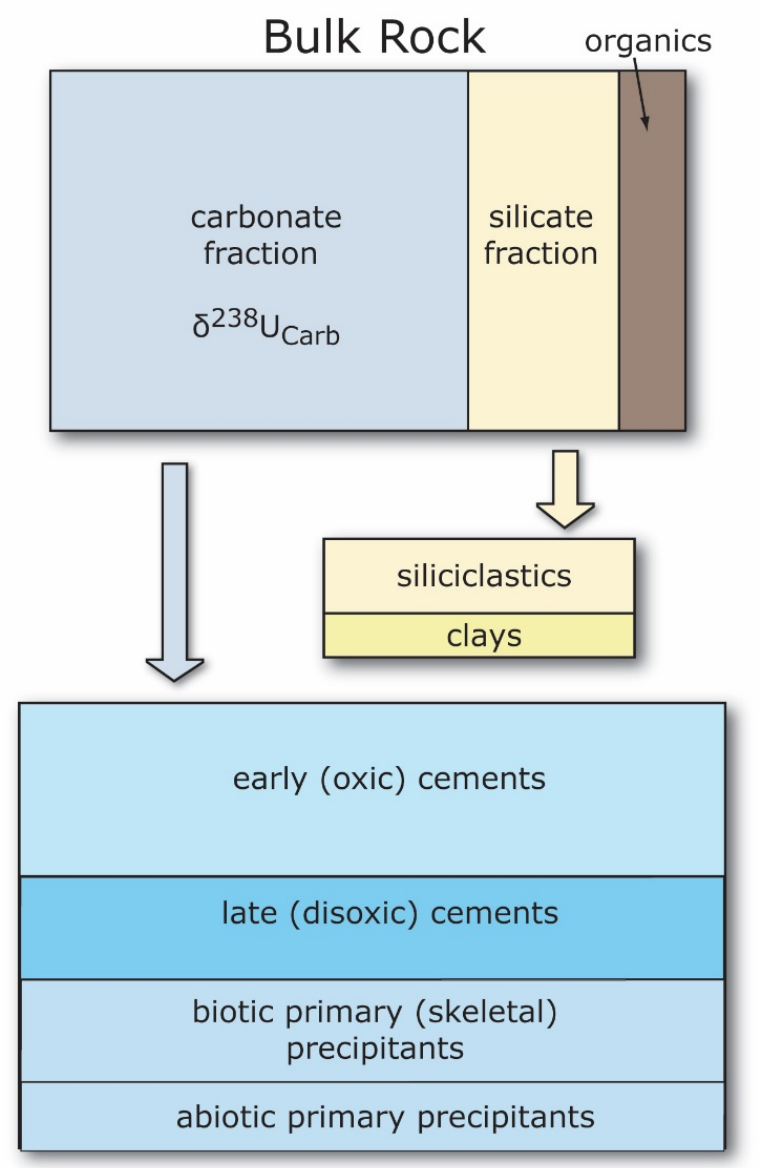

Supplemental Figure 6. Box model of the various $\delta^{238}U$ signals contained within a given marine carbonate whole rock sample. Unshaded boxes in the carbonate fraction represent the $\delta^{238}U$ of the ocean whereas the dark blue represent values potentially more positive that ocean $\delta^{238}U$.

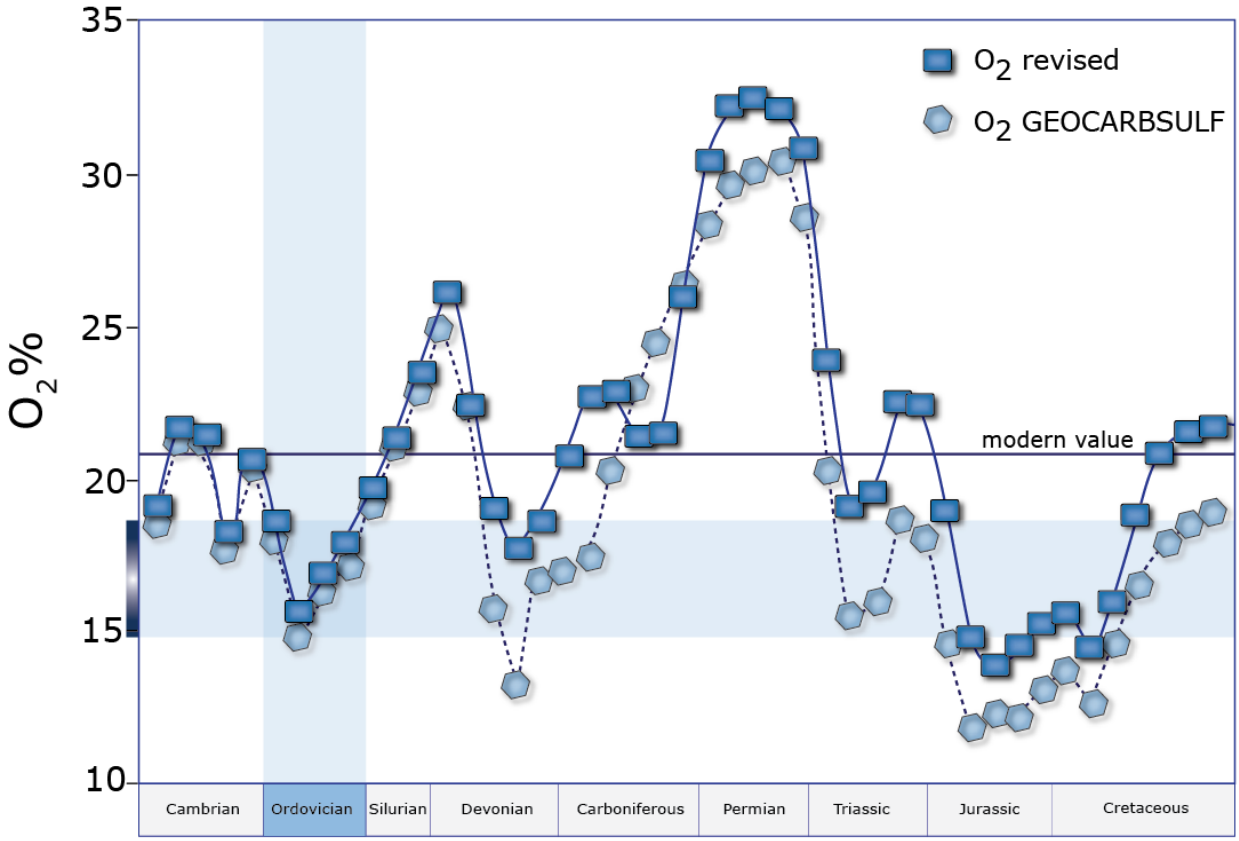

Supplemental Figure 7. Atmospheric oxygen through the Phanerozoic, adapted from Berner, 1994; 2009.

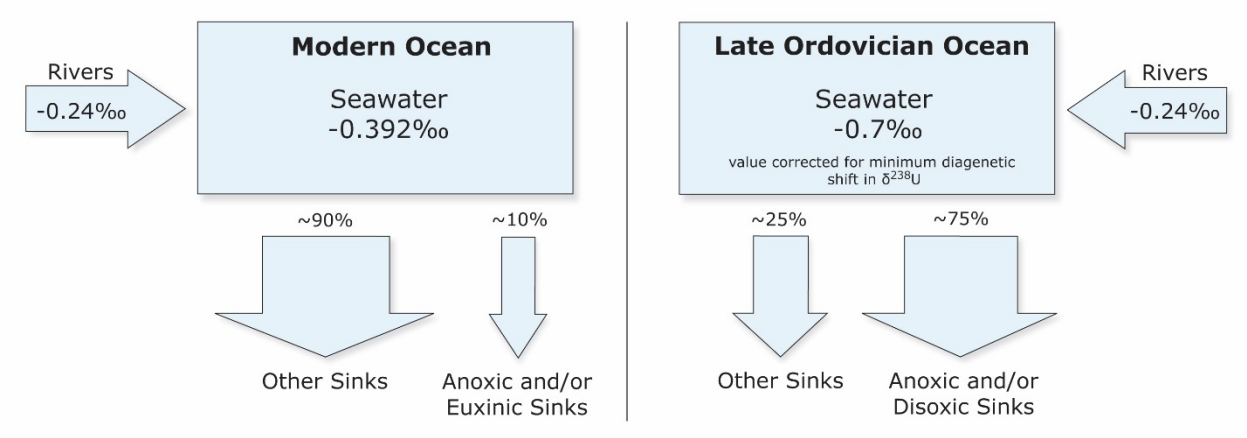

$\delta^{238}U_{rivers} = (A * a) + (B * b) + (C * c) + (D * d)$ where:

A = δ^{238}U oxic sinks	B = δ^{238}U dysoxic sinks	C = δ^{238}U anoxic sinks	D = δ^{238}U altered basalt sinks
a = percent of global deposition occurring under oxic conditions	*b* = percent of global deposition occurring under dysoxic conditions	*c* = percent of global deposition occurring under anoxic conditions	*d* = percent of global deposition occurring under hydrothermal settings

Supplemental Figure 8. Box model showing a possible solution to the mass balance equation for U in the Ordovician ocean. Values for percent of deposition occurring under anoxic conditions much higher than today are needed to match the observed δ^{238}U of the Late Ordovician. The value of the Ordovician ocean is equal to that measured in the Anticosti section (~-0.45 ‰) plus a correction of ~- 0.25 ‰. This correction is explained in Figure 9. NOTE: It is important to remember that the percentages represent the relative amounts of U being removed under a given redox condition and do not reflect percentages of the ocean or areas.

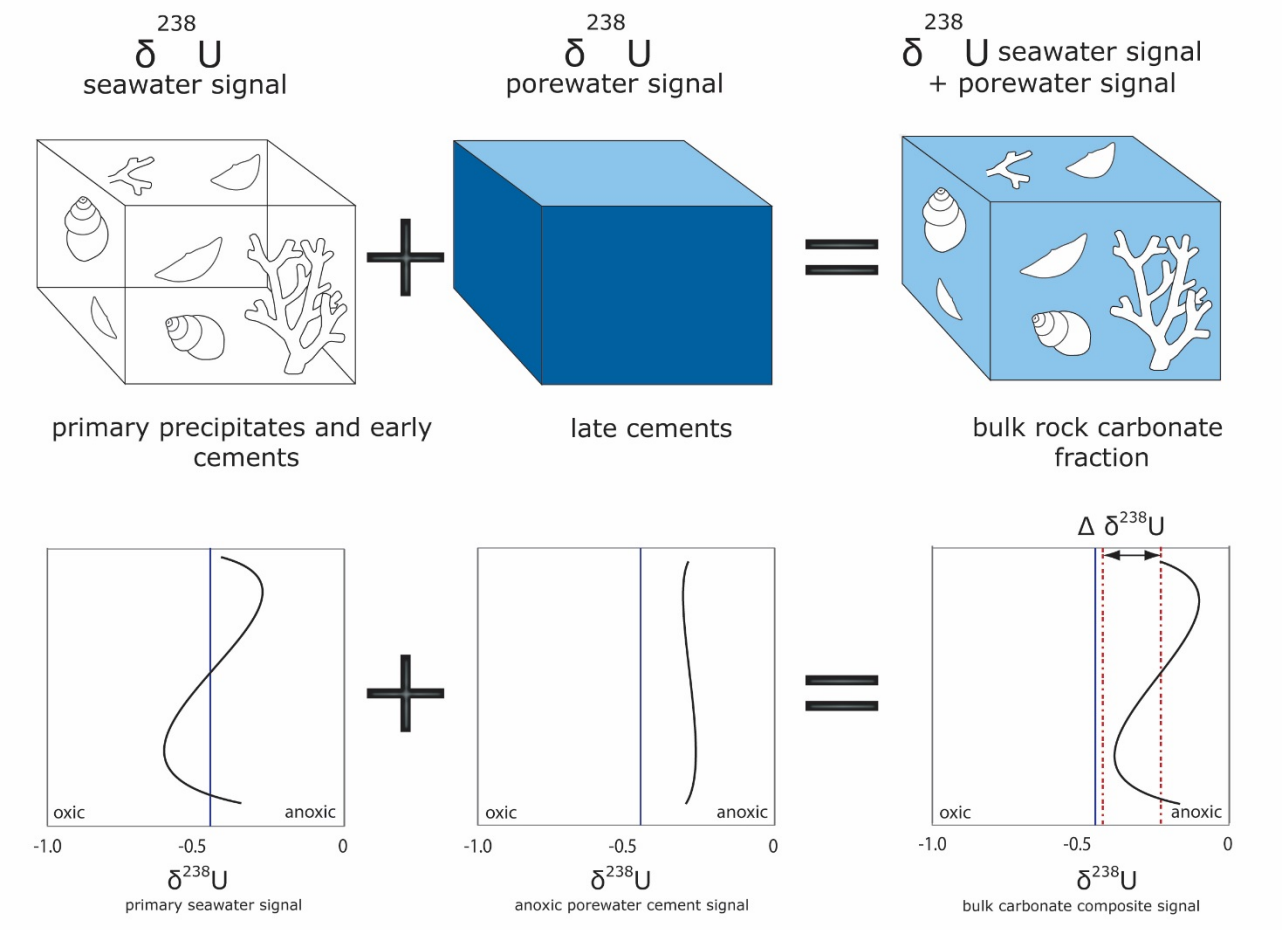

Supplemental Figure 9. The $\delta^{238}U$ signal of a bulk carbonate sample represents the combination of at least two components. The signal of the primary precipitates reflecting ambient seawater $\delta^{238}U$ plus the $\delta^{238}U$ of any porewater cements precipitated during diagenesis or later due to alteration. The $\delta^{238}U$ of such cements may not be the same as that of seawater because of the preferential incorporation of ^{238}U from anoxic pore waters. Graphs show a hypothetical primary seawater signal (left), the signal of cements precipitated under anoxic/euxinic conditions (middle) and the composite signal measured in bulk carbonates (right). The composite signal (right) reflects variations in the $\delta^{238}U$ of the ocean; it is however shifted toward higher $\delta^{238}U$ values by $\Delta\delta^{238}U$ imparted by porewater cements.

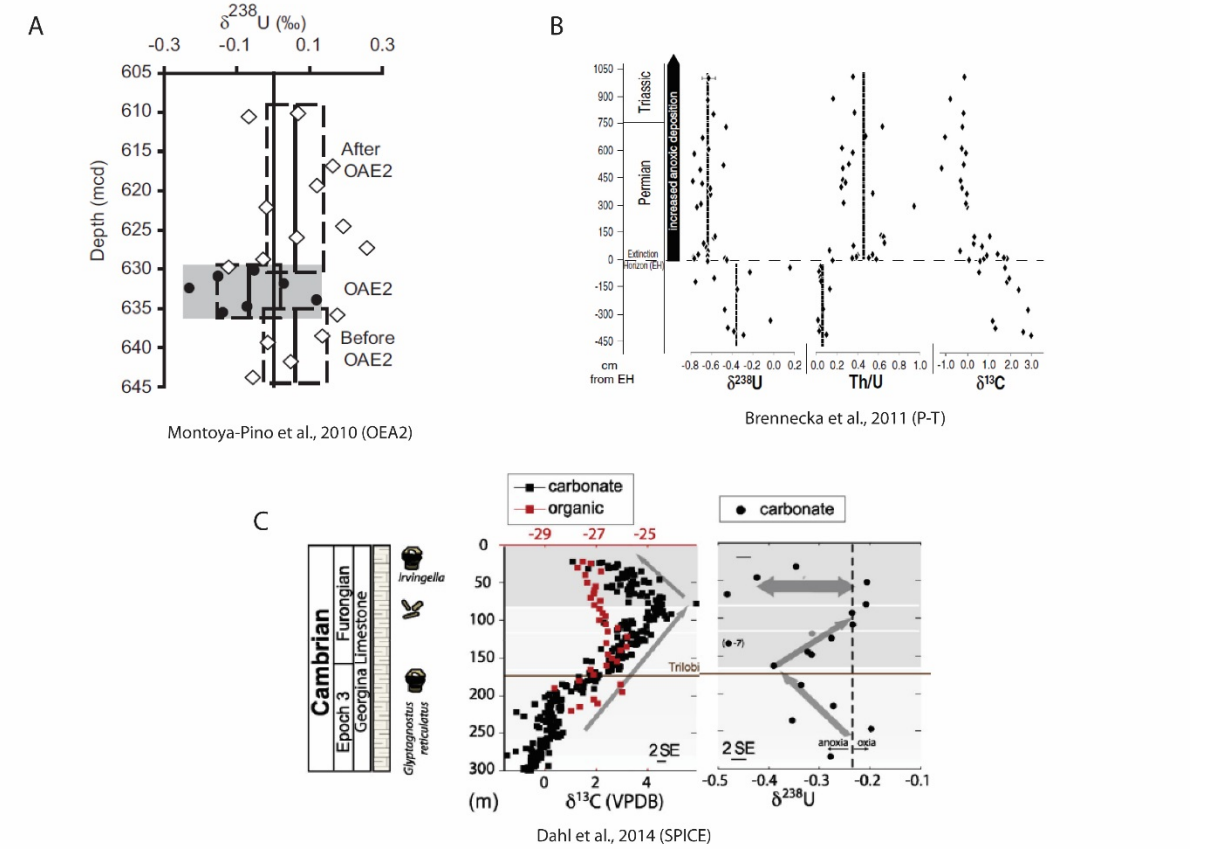

Source	$\delta^{238}U$ values	Duration	Δ anoxic deposition compared to modern	Magnitude of negative $\delta^{238}U$ excursion
A.) Montoya-Pino et al., 2010 (OAE2)	0.4 → –0.55 ‰	400-600 Ky	2-6 fold	-0.11 ‰
B.) Brennecka et al., 2011 (LPME)	−0.37 → −0.65 ‰	NA	6 fold	-0.28 ‰
C.) Dahl et al., 2014 (SPICE)	−0.21 → -0.39 ‰	1.2-1.7Ma	3-5 fold	-0.18 ‰
This study	-0.25 → -0.6 ‰	~550 Ky	7 fold	-0.35 ‰

Supplemental Figure 10. Results from previous studies.

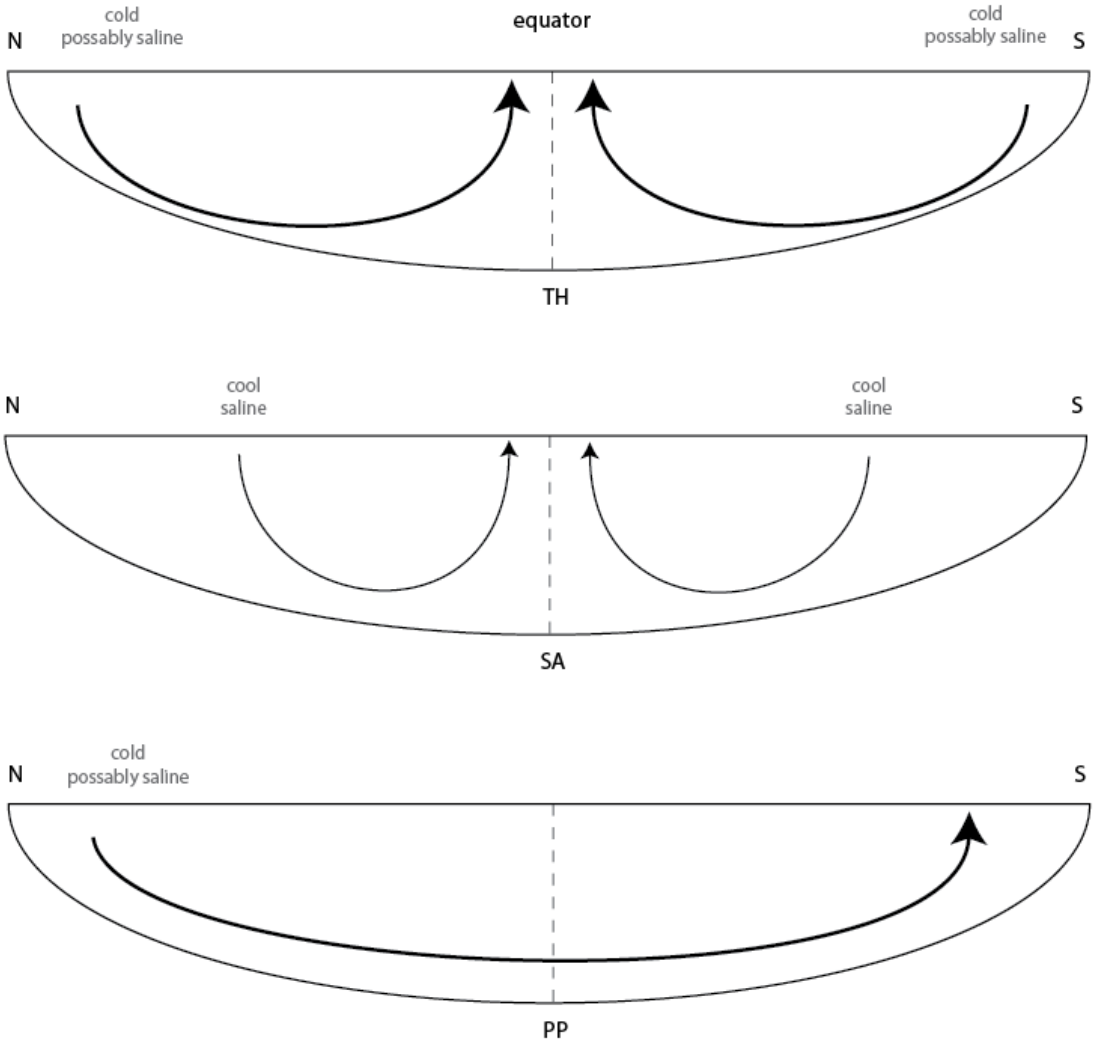

Supplemental Figure 11. Diagram showing the three stable global thermohaline circulation models. Modified from Saravanan and McWilliams (1995) and Thual and McWilliams, J.C., (1992).

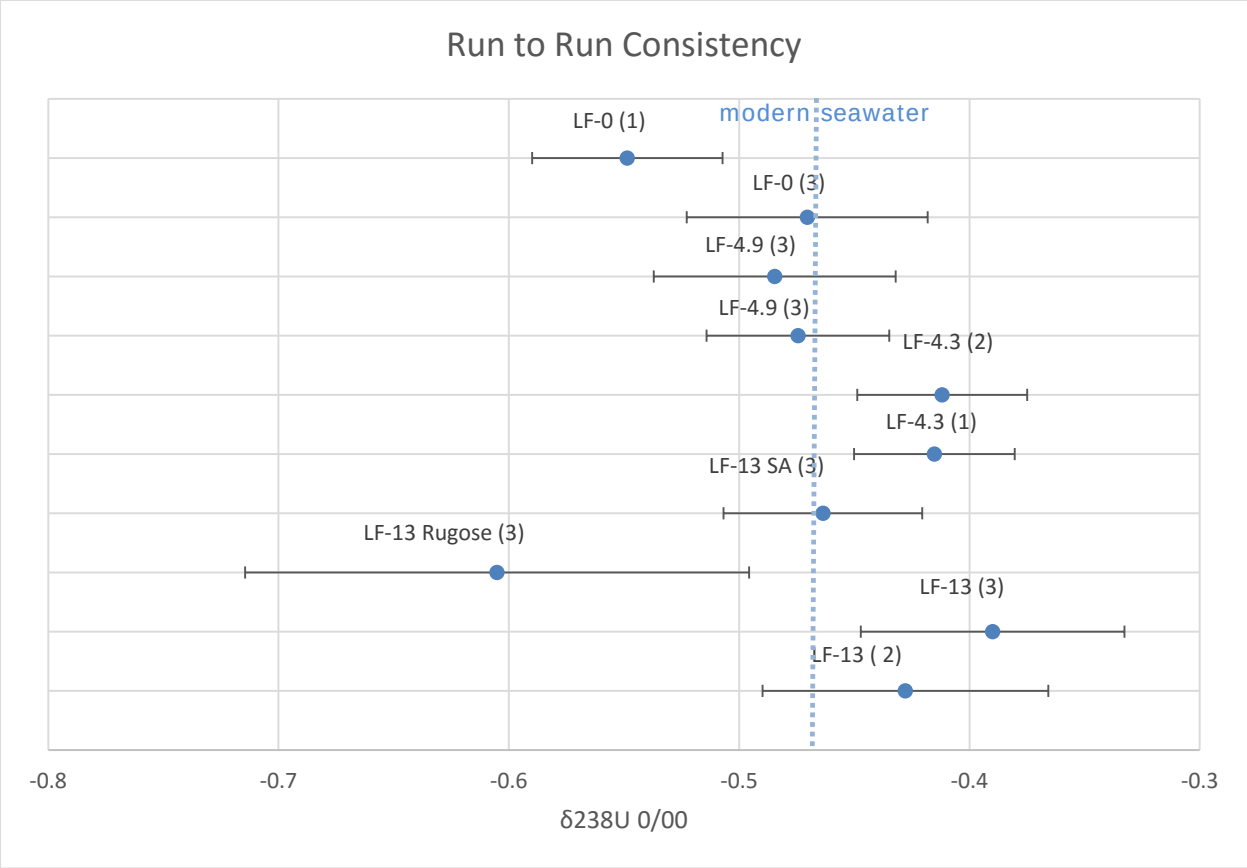

Supplemental Figure 12. Run to run consistency. () indicate batch number. ***PP*** *= Primary Precipitate (Rugose coral)* ***SA*** *= (strong acid, 6 N HCl)* ***N*** *= normal 1 N acetic acid.*

	Sample ID	Strat Level	$\delta^{238}U_{carb}$	2sigma	U_{carb} ppm	Th/U_{carb}	TOC	% Carbonate
46	507	238	***	***	0.27954	1.94	0.19	70
47	496	231	***	***	0.19473	2.71	0.24	79
44	EM-46	230	0.438	0.1179	***	***	***	***
43	EM-45	229	0.107	0.0922	***	***	0.18	***
45	EM-44	228	2.688	0.1404	0.03239	***	***	88
48	EM 44	228	***	***	***	1.43	***	***
49	481	221	***	***	***	0.73	0.15	96
1	481	221	-0.517	0.0570	0.34886	***	***	***
2	474	217	-0.421	0.0558		0.35	***	***
3	LF(22.7)	216	-0.350	0.0344	0.03963	***	0.17	***
50	LF-22.7	216	***	***	***	1.15	0.17	88
4	LT(21.5)	215	-0.302	0.0348	***	***	***	***
5	LF(20.5)	214	-0.309	0.0543	***	***	***	***
6	LF(19.7)	213	-0.382	0.0464	***	***	***	***
7	LT(18.4)	211	-0.158	0.0401	0.64277	***	***	94
51	LF 18.4	211	***	***	***	0.34	***	94
8	LF(17.4)	210	-0.341	0.0422	***	***	0.18	***
9	LT(16.4)	209	-0.307	0.0501	***	***	***	***
10	LT(15.4)	208	-0.425	0.0404	***	***	***	***
11	LF(14.8)	208	-0.522	0.0584	***	***	***	***
12	LT(13.8)	207	-0.326	0.0707	***	***	***	***
13	LF(13.8)	207	-0.405	0.0387	0.08328	***	***	***
14	LF(13)	206	-0.428	0.0620	***	***	0.12	***
15	LF(13) N	206	-0.390	0.0572	0.27389	2.83	***	***
16	LF(13) PP	206	-0.605	0.1095	***	***	***	***
17	LF(13) SA	206	-0.464	0.0431	***	***	***	***
52	LF 13	206			***	***	***	***
18	LF(12.3)	205	-0.793	0.0440	***	***	0.15	***
53	LF 12.3	205			***	0.47	0.15	***
19	LF(12)	205	-0.790	0.0307	***	***	0.16	***
20	LF(11.5)	205	-0.485	0.0525	***	***	0.22	75
54	LF 11.5	205			0.10521	4.19	0.22	***
21	LF(10.7)	204	-0.320	0.0734	***	***	0.51	66
22	LF(10)	203	-0.280	0.0554	***	***	0.15	***
23	LF(9)	202	-0.405	0.0167	***	***	0.56	***
24	LF(5.7)	199	-0.410	0.0369	0.05791	***		82
55	LF 5.7	199			***	1.20	0.58	***
25	LF(4.3)b	198	-0.412	0.0368	***	***	***	***
26	LF(4.9)	198	-0.474	0.0397	***	***	0.19	78
27	LF(4.9)	198	-0.485	0.0525	***	***	0.19	***
28	LF(4.3)	197	-0.415	0.0348	0.42936	***	***	***
29	LF(3)	196	-0.494	0.0607	***	***	***	***
30	LF(2.3)	195	-0.443	0.0669	***	***	***	90
31	LF(1.3)	194	-0.495	0.0582	0.27225	***	***	91
32	LF(0)	193	-0.549	0.0414	0.30718	3.56		82
33	LF(0) re-run	193	-0.470	0.0523		***	***	***
34	LF(-1)	192	-0.564	0.0747	0.72469	***	***	***
36	LF(-3)	191	-0.575	0.1352	0.19334	***	***	***
35	LF(-2)	190	-0.838	0.0798	0.2826	***	***	***
37	LM-60	190	-0.245	0.1032	0.04068	1.81	***	***
56	LM 60	190	***	***	***	***	***	***
38	LM-51	175	-0.004	0.0913	0.06252	***	0.18	92
57	LM 51	175	***	***	***	0.55	0.18	92
39	LM-43	161	-0.081	0.0816	***	***	0.23	80
58	LM 43	161	***	***	0.26812	4.14	0.23	80
40	356	149	-0.889	0.0529	0.3977	0.72	0.19	85
41	PC	128	-0.232	0.1349	***	***	0.15	92
61	318	127	***	***	0.53339	0.85	0.19	***
60	296	112	***	***	0.26588	3.25	0.13	61
62	292	104	***	***	***	0.30	0.13	***
42	265	87	-0.502	0.0422	0.66041	0.88	0.23	88
64	240	71	***	***	***	1.04	0.20	***
66	223	60	***	***	***	***	0.12	***
65	201	45	***	***	0.22475	0.92	0.16	97
67	CV-5.3	39	-2.153	0.1215	***	***	***	***
68	CV-8.6	39	-3.953	0.1397	***	***	***	***
69	CVB-1.0	38	-4.046	0.1243	***	***	***	***
AVG			-0.5254	0.0662	0.2800	1.6079	0.2127	84.3511
Median			-0.423	0.056	0.270	1.095	0.184	87.592
Std Dev			0.914	0.033	0.198	1.236	0.113	9.387

Supplemental Table 1. Data for this study.

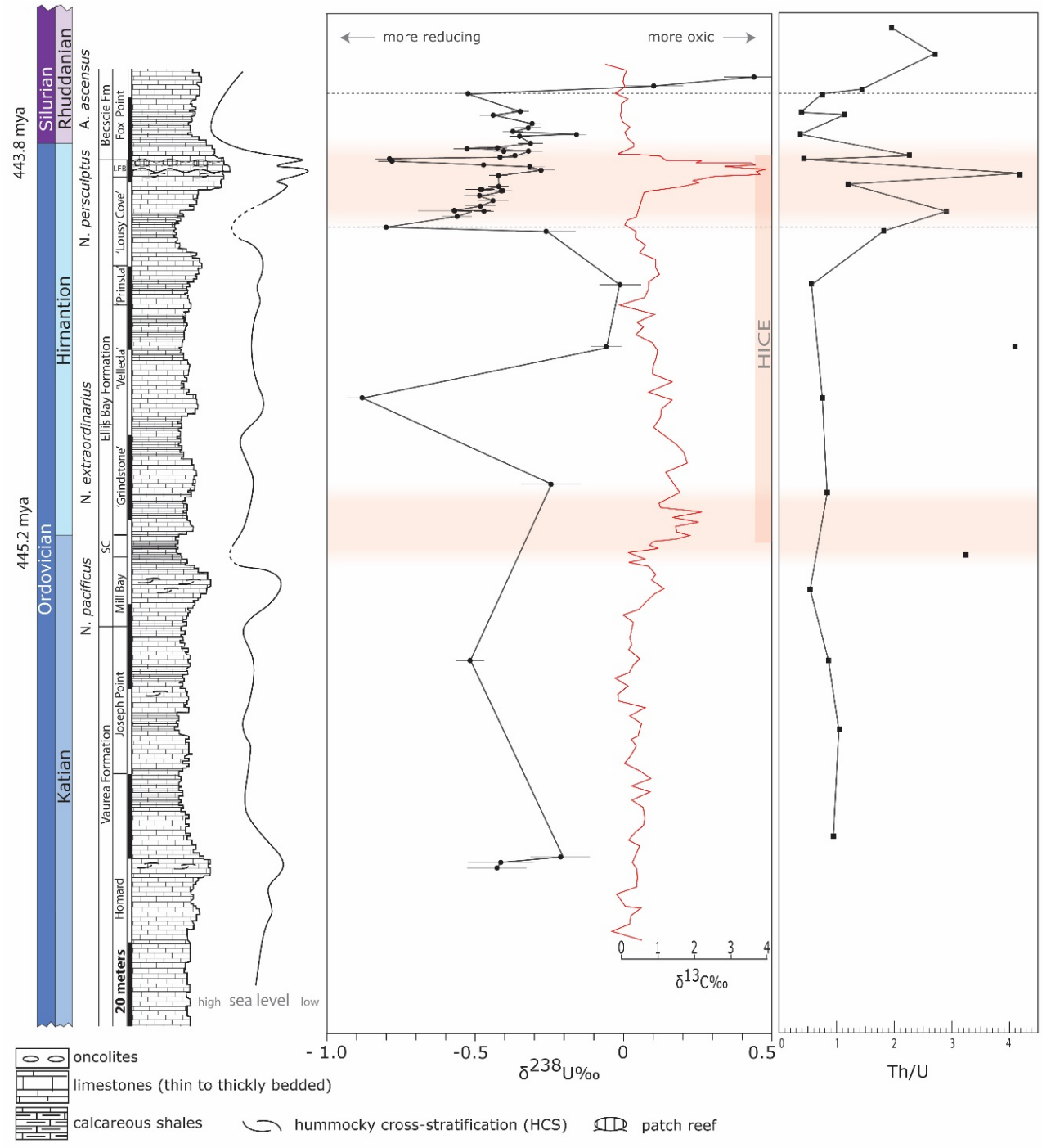
443.8 mya
445.2 mya
Silurian
Rhuddanian
Ordovician
Hirnantion
Katian
A. ascensus
N. persculptus
N. extraordinarius
N. pacificus
Beccscie Fm
Fox Point
LF3
'Lousy Cove'
Prinsta
Ellis Bay Formation
'Velleda'
'Grindstone'
SC
Mill Bay
Joseph Point
Vaurea Formation
Homard
20 meters
high sea level low
more reducing
more oxic
HICE
δ13C‰
δ238U‰
Th/U
oncolites
limestones (thin to thickly bedded)
calcareous shales
hummocky cross-stratification (HCS)
patch reef

References

Achab, A., Asselin, E., Desrochers, A., Riva, J.F., 2013. The end-Ordovician chitinozoan zones of Anticosti Island, Québec: Definition and stratigraphic position. Rev. Palaeobot. Palynol. 198, 92–109. doi:10.1016/j.revpalbo.2012.07.019

Alroy, J., Aberhan, M., Bottjer, D.J., Foote, M., Fursich, F.T., Harries, P.J., Hendy, A.J.W., Holland, S.M., Ivany, L.C., Kiessling, W., Kosnik, M.A., Marshall, C.R., McGowan, A.J., Miller, A.I., Olszewski, T.D., Patzkowsky, M.E., Peters, S.E., Villier, L., Wagner, P.J., Bonuso, N., Borkow, P.S., Brenneis, B., Clapham, M.E., Fall, L.M., Ferguson, C.A., Hanson, V.L., Krug, A.Z., Layou, K.M., Leckey, E.H., Nurnberg, S., Powers, C.M., Sessa, J.A., Simpson, C., Tomasovych, A., Visaggi, C.C., 2008. Phanerozoic Trends in the Global Diversity of Marine Invertebrates. Science 321, 97–100.

Andersen, M.B., Romaniello, S.J., Vance, D., Little, S.H., Herdman, R., Lyons, T.W., 2014. A modern framework for the interpretation of 238U/235U in studies of ancient ocean redox. Earth Planet. Sci. Lett. 400, 184–194. doi:10.1016/j.epsl.2014.05.051

Armstrong, H.A., Coe, A.L., 1997. Deep-sea sediments record the geophysiology of the late Ordovician glaciation. J. Geol. Soc. London. 154, 929–934. doi:10.1144/gsjgs.154.6.0929

Arthur, M.A., Sageman, B.B., 1994. Marine shales: depositional mechanisms and environments of ancient deposits. Annual Review of Earth and Planetary Sciences, 22, 499-551.

Asael, D., Tissot, F.L.H., Reinhard, C.T., Rouxel, O., Dauphas, N., Lyons, T.W., Ponzevera, E., Liorzou, C., Chéron, S., 2013. Coupled molybdenum, iron and uranium stable isotopes as oceanic paleoredox proxies during the Paleoproterozoic Shunga Event. Chem. Geol. 362, 193–210. doi:10.1016/j.chemgeo.2013.08.003

Barnes, C.E., Cochran, J.K., 1993. Uranium geochemistry in estuarine sediments: Controls on removal and release processes. Geochim. Cosmochim. Acta 57, 555–569. doi:10.1016/0016-7037(93)90367-6

Bergman, N.M., Lenton, T.M., Watson, A.J., 2004. COPSE: A new model of biogeochemical cycling over phanerozoic time. Am. J. Sci. 304, 397–437. doi:10.2475/ajs.304.5.397

Bergstrom, S.M., Saltzman, M.M., Schmitz, B., 2006. First record of the Hirnantian (Upper Ordovician) δ13C excursion in the North American Midcontinent and its regional implications. Geol. Mag. 143, 657. doi:10.1017/S0016756806002469

Berner, R.A., 2009. Phanerozoic atmospheric oxygen: new results using the geocarbsulf model. Am. J. Sci. 309, 603–606. doi:10.2475/07.2009.03

Berner, R.A., 2006. GEOCARBSULF: a combined model for Phanerozoic atmospheric O2 and CO2. Geochim. Cosmochim. Acta 70, 5653-5664.

Berner, R.A., 1994. GEOCARB II: A revised model of atmospheric CO2 over Phanerozoic time. Am. J. Sci. 294, 56–91.

Berner, R.A., Kothavala, Z., 2001. GEOCARB III: A revised model of atmospheric CO2 over Phanerozoic time. Am. J. Sci. 301, 182–204. doi:10.2475/ajs.294.1.56

Berry, W.B.N., Wilde, P., 1978. Progressive ventilation of the oceans - An explanation for the distribution of the lower Paleozoic black shales. Am. J. Sci. 278, 257–275.

Berry, W.B.N., Wilde, P., Quinby-Hunt, M.S., 1990. Late Ordovician graptolite mass mortality and subsequent early Silurian re-radiation. Extinction Events in Earth History. Springer Berlin Heidelberg, 115-123.

Bigeleisen, J., 1996a. Temperature dependence of the isotope chemistry of the heavy elements. Proc. Natl. Acad. Sci. 93, 9393–9396. doi:10.1073/pnas.93.18.9393

Blakey, R.C., 2014. Colorado Plateau Geosystems [WWW Document]. URL http://cpgeosystems.com/index.html

Brenchley, P.J., 2001. Late Ordovician extinction, in: Palaeobiology II. Blackwell Science Ltd., Malden, MA, p. 22. doi:10.1002/9780470999295.ch46

Brenchley, P.J., 1994. Bathymetric and isotopic evidence for a short-lived late Ordovician glaciation in a greenhouse period. Geology 22, 295–298. doi:10.1130/0091-7613(1994)022<0295:BAIEFA>2.3.CO

Brenchley, P.J., Carden, G.A., Hints, L., Kaljo, D., Marshall, J.D., Martma, T., Meidla, T., Nõlvak, J., 2003. High-resolution stable isotope stratigraphy of Upper Ordovician sequences: Constraints on the timing of bioevents and environmental changes associated with mass. Geol. Soc. Am. Bull. 115, 89–104. doi:10.1130/0016-7606(2003)115<0089

Brennecka, G.A., Herrmann, A.D., Algeo, T.J., Anbar, A.D., 2011. Rapid expansion of oceanic anoxia immediately before the end-Permian mass extinction. Proc. Natl. Acad. Sci. 108, 17631–17634. doi:10.1073/pnas.1106039108

Buggisch, W., Joachimski, M.M., Lehnert, O., Bergstrom, S.M., Repetski, J.E., Webers, G.F., 2010. Did intense volcanism trigger the first Late Ordovician icehouse? Geology, 38, 327–330, doi:10.1130/G30577.1

Canfield, D.E., 1998. A new model for Proterozoic ocean chemistry. Nature 396, 450-453.

Chen, J.H., Edwards, R.L., Wasserburg, G.J., 1986. 238U 234U and 232Th in seawater. Earth Planet. Sci. Lett. 80, 241–251.

Cocks, L.R.M., Torsvik, T.H., 2004. Major terranes in the Ordovician, in: The Great Ordovician Biodiversification Event. Columbia University Press, New York, pp. 61–67.

Cohen, K.M., Finney, S.C., Gibbard, P.L., Fan, J.X., 2013. The ICS International Chronostratigraphic Chart: Episodes 36: 199-204 [WWW Document]. URL http://www.stratigraphy.org/index.php/ics-chart-timescale

Copper, P., Jin, J., 2014. The revised Lower Silurian (Rhuddanian) Becscie Formation, Anticosti Island, eastern Canada records the tropical marine faunal recovery from the end-Ordovician Mass Extinction. Newsletters Stratigr. 47, 61–83. doi:10.1127/0078-0421/2014/0040

Cramer, B.D., Saltzman, M.R., 2005. Sequestration of 12C in the deep ocean during the early Wenlock (Silurian) positive carbon isotope excursion. Palaeogeogr. Palaeoclimatol. Palaeoecol. 219, 333–349. doi:10.1016/j.palaeo.2005.01.009

Dahl, T.W., Boyle, R.A., Canfield, D.E., Connelly, J.N., Gill, B.C., Lenton, T.M., Bizzarro, M., 2014. Uranium isotopes distinguish two geochemically distinct stages during the later Cambrian SPICE event. Earth Planet. Sci. Lett. 401, 313–326. doi:10.1016/j.epsl.2014.05.043

Dahl, T.W., Hammarlund, E.U., Anbar, A.D., Bond, D.P.G., Gill, B.C., Gordon, G.W., Knoll, A.H., Nielsen, A.T., Schovsbo, N.H., Canfield, D.E., 2010. Devonian rise in atmospheric oxygen correlated to the radiations of terrestrial plants and large predatory fish. Proc. Natl. Acad. Sci. U. S. A. 107, 17911–17915. doi:10.1073/pnas.1011287107

Desrochers, A., Farley, C., Achab, A., Asselin, E., Riva, J.F., 2010. A far-field record of the end Ordovician glaciation: The Ellis Bay Formation, Anticosti Island, Eastern Canada. Palaeogeogr. Palaeoclimatol. Palaeoecol. 296, 248–263. doi:10.1016/j.palaeo.2010.02.017

Djogic, R., 1986. Characterization of uranium (V1) in seawater . Liminology Oceanogr. 31.

Droser, M.L., Bottjer, D.J., Sheehan, P.M., McGhee Jr., G.R., 2000. Decoupling of taxonomic and ecologic severity of Phanerozoic marine mass extinctions. Geology 28, 675–678. doi:10.1130/0091-7613(2000)28<675:DOTAES>2.0.CO

Droser, M.L., Finnegan, S., 2003. The Ordovician Radiation: A Follow-up to the Cambrian Explosion? Integr. Comp. Biol. 43, 178–184. doi:10.1093/icb/43.1.178

Dunk, R.M., Mills, R.A., Jenkins, W.J., 2002. A reevaluation of the oceanic uranium budget for the Holocene. Chem. Geol. 190, 45–67. doi:10.1016/S0009-2541(02)00110-9

Finnegan, S., Bergmann, K., Eiler, J.M., Jones, D.S., Fike, D.A., Eisenman, I., Hughes, N.C., Tripati, A.K., Fischer, W.W., 2011. The Magnitude and Duration of Late Ordovician – Early Silurian Glaciation. Science 3, 903–906.

Finnegan, S., Heim, N.A., Peters, S.E., Fischer, W.W., 2012. Climate change and the selective signature of the Late Ordovician mass extinction. Proc. Natl. Acad. Sci. 109, 6829–6834. doi:DOI 10.1073/pnas.1117039109

Finney, S.C., Berry, W.B.N., Cooper, J.D., Ripperdan, R.L., Sweet, W.C., Jacobson, S.R., Soufiane, A., Achab, A., Noble, P.J., 1999. Late Ordovician mass extinction: A new perspective from stratigraphic sections in central Nevada. Geology 27, 215–218. doi:10.1130/0091-7613(1999)027<0215:LOMEAN>2.3.CO;2

Fischer, A.G., Arthur, M.A., 1977. Secular variations in the pelagic realm. Deep-Water Carbonate Environments: Tulsa, 19–50.

Fortey, R.A., 1989. There are extinctions and extinctions: examples from the lower Paleozoic. Philosophical Transactions of the Royal Society of London Series B: Biological Sciences 325, 327–355.

Ghienne, J.F., Desrochers, A., Vandenbroucke, T.R.A., Achab, A., Asselin, E., Dabard, M.P., Farley, C., Loi, A., Paris, F., Wickson, S., Veizer, J., 2014. A Cenozoic-style scenario for the end-Ordovician glaciation. Nat. Commun. 5, 4485. doi:10.1038/ncomms5485

Goodfellow, W.D., Jonasson, I.R., 1984. Ocean stagnation and ventilation defined by d-34S secular trends in pyrite and barite, Selwyn Basin, Yukon. Geology 12, 583–586. doi:10.1130/0091-7613(1984)12<583:OSAVDB>2.0.CO;2

Hammarlund, E.U., Dahl, T.W., Harper, D.A.T., Bond, D.P.G., Nielsen, A.T., Bjerrum, C.J., Schovsbo, N.H., Schonlaub, H.P., Zalasiewicz, J.A., Canfield, D.E., 2012. A sulfidic driver for the end-Ordovician mass extinction. Earth Planet. Sci. Lett. 331-332, 128–139. doi:10.1016/j.epsl.2012.02.024

Harper, D.A.T., 2006. The Ordovician biodiversification: Setting an agenda for marine life. Palaeogeogr. Palaeoclimatol. Palaeoecol. 232, 148–166.

Harper, D.A.T., Hammarlund, E.U., Rasmussen, C.M.O., 2013. End Ordovician extinctions: A coincidence of causes. Gondwana Res. 25, 1294–1307. doi:10.1016/j.gr.2012.12.021

Henderson, G.M., Anderson, R.F., 2003. The U-series toolbox for paleoceanography. Rev. Mineral. Geochemistry 52, 493–531. doi:10.2113/0520493

Hotinski, R.M., Bice, K.L., Kump, L.R., Najjar, R.G., Arthur, M.A., 2001. Ocean stagnation and end-Permian anoxia. Geology, 29, 7-10.

Ingall, E.D., Bustin, R.M., Van Cappellen, P., 1993. Influence of water column anoxia on the burial and preservation of carbon and phosphorus in marine shales. Geochim. Cosmochim. Acta 57, 303–316. doi:10.1016/0016-7037(96)00041-5

Ivanovich, M., Harmon, R.S., 1992. Uranium-series Disequilibrium: Applications to Earth, Marine, and Environmental Sciences, 2nd ed. Clarendon Press, University of California.

Jablonski, D., 1991. Extinctions: a paleontological perspective. Science, 253, 754.

Jenkyns, H.C., 2010. Geochemistry of oceanic anoxic events. Geochemistry, Geophys. Geosystems 11, 1–30. doi:10.1029/2009GC002788

Jones, B., Manning, D., 1994. Comparison of geochemical indices used for the interpretation of palaeoredox conditions in ancient mudstones. Chemical Geology 1, 111-129.

Kasting, J.F., Howard, M.T., Wallmann, K., Veizer, J., Shield, G., Jaffres, J., 2006. Paleoclimates, ocean depth, and the oxygen isotopic composition of seawater. Geochim. Cosmochim. Acta 70, A307. doi:10.1016/j.gca.2006.06.622

Klinkhammer, G.P., Palmer, M.R., 1991. Uranium in the oceans: Where it goes and why. Geochim. Cosmochim. Acta 55, 1799–1806. doi:10.1016/0016-7037(91)90024-Y

Ku, T.L., Knauss, K.G., Mathieu, G.G., 1977. Uranium in open ocean: concentration and isotopic composition. Deep. Res. 24, 1005–1017.

Kump, L.R., Arthur, M.A., Patzkowsky, M.E., Gibbs, M.T., Pinkus, D.S., Sheehan, P.M., 1999. A weathering hypothesis for glaciation at high atmospheric pCO2 during the Late Ordovician. Palaeogeogr. Palaeoclimatol. Palaeoecol. 152, 173–187. doi:10.1016/S0031-0182(99)00046-2

Lau, K. V., Maher, K., Altiner, D., Kelley, B.M., Kump, L.R., Lehrmann, D.J., Silva-Tamayo, J.C., Weaver, K.L., Yu, M., Payne, J.L., 2016. Marine anoxia and delayed Earth system recovery after the end-Permian extinction. Proc. Natl. Acad. Sci. U. S. A. 113, 2360–2365. doi:10.1073/pnas.1515080113

Leckie, R.M., Bralower, T.J., Cashman, R., 2002. Oceanic anoxic events and plankton evolution: Biotic response to tectonic forcing during the mid-Cretaceous. Paleoceanography 17, 13–1–13–29. doi:10.1029/2001PA000623

Lenton, T.M., Crouch, M., Johnson, M., Pires, N., Dolan, L., 2012. First plants cooled the Ordovician. Nature Geoscience, 5, 86-89.

Long, D.G.F., 2007. Tempestite frequency curves: a key to Late Ordovician and Early Silurian subsidence, sea-level change, and orbital forcing in the Anticosti foreland basin, Quebec, Canada. Can. J. Earth Sci. 44, 413–431.

Mauviel, A., Desrochers, A., 2016. A high-resolution, continuous d13C record spanning the Ordovician–Silurian boundary on Anticosti Island, eastern Canada. Can. J. Earth Sci. 53, 1–7.

McGhee, G.R., Sheehan, P.M., Bottjer, D.J., Droser, M.L., 2012. Ecological ranking of Phanerozoic biodiversity crises: the Serpukhovian (early Carboniferous) crisis had a greater ecological impact than the end-Ordovician. Geology, 40, 147-150.

McGhee Jr., G.R., Sheehan, P.M., Bottjer, D.J., Droser, M.L., 2004. Ecological ranking of Phanerozoic biodiversity crises: Ecological and taxonomic severities are decoupled. Palaeogeogr. Palaeoclimatol. Palaeoecol. 211, 289–297. doi:10.1016/j.palaeo.2004.05.010

McManus, J., Berelson, W.M., Severmann, S., Poulson, R.L., Hammond, D.E., Klinkhammer, G.P., Holm, C., 2006. Molybdenum and uranium geochemistry in continental margin

sediments: Paleoproxy potential. Geochim. Cosmochim. Acta 70, 4643–4662. doi:10.1016/j.gca.2006.06.1564

Melchin, M.J., Mitchell, C.E., Holmden, C., Storch, P., 2013. Environmental changes in the Late Ordovician-early Silurian: Review and new insights from black shales and nitrogen isotopes. Geol. Soc. Am. Bull. 125, 1635–1670. doi:10.1130/B30812.1

Melott, A.L., Thomas, B.C., 2009. Late Ordovician geographic patterns of extinction compared with simulations of astrophysical ionizing radiation damage. Paleobiology, 35, 311-320.

Melott, A.L., Lieberman, B.S., Laird, C.M., Martin, L.D., Medvedev, M.V., Thomas, B.C., Cannizzo, J.K., Gehrels, N., Jackman, C.H., 2004. Did a gamma-ray burst initiate the late Ordovician mass extinction? International Journal of Astrobiology, 3, 55-61.

Meyer, K.M., Kump, L.R., 2008. Oceanic euxinia in Earth history: causes and consequences. Annu. Rev. Earth Planet. Sci., 36, 251-288.

Montoya-Pino, C., Weyer, S., Anbar, A.D., Pross, J., Oschmann, W., van de Schootbrugge, B., Arz, H.W., 2010. Global enhancement of ocean anoxia during oceanic anoxic event 2: A quantitative approach using U isotopes. Geology 38, 315–318. doi:10.1130/G30652.1

Morford, J.L., Emerson, S., 1999. The geochemistry of redox sensitive trace metals in sediments. Geochim. Cosmochim. Acta 63, 1735–1750. doi:10.1016/S0016-7037(99)00126-X

Morford, J.L., Emerson, S.R., Breckel, E.J., Kim, S.H., 2005. Diagenesis of oxyanions (V, U, Re, and Mo) in pore waters and sediments from a continental margin. Geochim. Cosmochim. Acta 69, 5021–5032. doi:10.1016/j.gca.2005.05.015

Morford, J.L., Martin, W.R., Carney, C.M., 2009. Uranium diagenesis in sediments underlying bottom waters with high oxygen content. Geochemica Cosmochem. Acta 73, 2920–2937.

Munnecke, A., Samtleben, C., Bickert, T., 2003. The Ireviken Event in the lower Silurian of Gotland, Sweden - Relation to similar Palaeozoic and Proterozoic events. Palaeogeogr. Palaeoclimatol. Palaeoecol. 195, 99–124. doi:10.1016/S0031-0182(03)00304-3

Nardin, E., Goddéris, Y., Donnadieu, Y., Le Hir, G., Blakey, R.C., Pucéat, E., Aretz, M., 2011. Modeling the early Paleozoic long-term climatic trend. Bull. Geol. Soc. Am. 123, 1181–1192. doi:10.1130/B30364.1

Nardin, E., Lefebvre, B., 2010. Unravelling extrinsic and intrinsic factors of the Early Palaeozoic diversification of blastozoan Echinoderms. Palaeogeogr. Palaeoclimatol. Palaeoecol. 294, 142–160.

Noordmann, J., Weyer, S., Montoya-Pino, C., Dellwig, O., Neubert, N., Eckert, S., Paetzel, M., Bottcher, M.E., 2015. Uranium and molybdenum isotope systematics in modern euxinic basins: Case studies from the central Baltic Sea and the Kyllaren fjord (Norway). Chem. Geol. 396, 182–195. doi:10.1016/j.chemgeo.2014.12.012

Page, A.A., Zalasiewicz, J.A., Williams, M., Popov, L.E., 2007. Were transgressive black shales a negative feedback mechanism modulating glacio-eustastic cycles in the Early Palaeozoic Icehouse?, in: Deep-Time Perspectives on Climate Change: Marrying the Signal from Computer Models and Biological Proxies. The Micropaleontological Society, Special Publications, London, pp. 123–156.

Petryk, A.A., 1981. Stratigraphy, Sedimentology and Paleogeography of the Upper Ordovician-Lower Silurian of Anticosti Island, Quebec. F. Meet. Anticosti-Gaspe 2, 11–39. doi:10.1017/CBO9781107415324.004

Rasmussen, C.M.O., Harper, D.A.T., 2011. Did the amalgamation of continents drive the end Ordovician mass extinctions? Palaeogeogr. Palaeoclimatol. Palaeoecol. 311, 48–62. doi:10.1016/j.palaeo.2011.07.029

Rohrssen, M., Love, G.D., Fischer, W.W., Finnegan, S., Fike, D.A., 2013. Lipid biomarkers record fundamental changes in the microbial community structure of tropical seas during the late ordovician hirnantian glaciation. Geology 41, 127–130. doi:10.1130/G33671.1

Romaniello, S.J., Herrmann, A.D., Anbar, A.D., 2013. Uranium concentrations and 238U/235U isotope ratios in modern carbonates from the Bahamas: Assessing a novel paleoredox proxy. Chem. Geol. 362, 305–316. doi:10.1016/j.chemgeo.2013.10.002

Sami, T., Desrochers, A., 1992. Episodic sedimentation on an early Silurian, storm-dominated carbonate ramp, Becscie and Merrimack formations, Anticosti Island, Canada. Sedimentology 39, 355–381. doi:10.1111/j.1365-3091.1992.tb02122.x

Saravanan, R., McWilliams, J.C., 1995. Multiple equilibria, natural variability, and climate transitions in an idealized ocean-atmosphere model. J. Clim. 8, 2296–2323.

Schauble, E.A., 2007. Role of nuclear volume in driving equilibrium stable isotope fractionation of mercury, thallium, and other very heavy elements. Geochim. Cosmochim. Acta 71, 2170–2189. doi:10.1016/j.gca.2007.02.004

Schlanger. S.O., Jenkyns, H.C., 1976. Cretaceous oceanic anoxic events: causes and consequences. Geol. Mijnb. 55, 179–84.

Sepkoski Jr., J.J., 1996. Patterns of Phanerozoic extinction: a perspective from global data bases, in: Global Events and Event Stratigraphy in the Phanerozoic. Springer-Verlag Berlin Heidelberg, pp. 35–51.

Servais, T., Owen, A.W., Harper, D.A.T., Kroger, B., Munnecke, A., 2010. The Great Ordovician Biodiversification Event (GOBE): The palaeoecological dimension.

Palaeogeogr. Palaeoclimatol. Palaeoecol. 294, 99–119. doi:10.1016/j.palaeo.2010.05.031

Sheehan, P.M., 2001. The Late Ordovician Mass Extinction. Annu. Rev. Earth Planet. Sci. 29, 331–364.

Sheehan, P.M., 2001a. The Late Ordovician mass extinction. Annual Review of Earth and Planetary Sciences 29, 331–364.

Sheehan, P.M., 2001b. History of marine diversity. Geological Journal 36, 231–249.

Sheehan, P.M., 2008. Did incumbency play a role in maintaining boundaries between Late Ordovician brachiopod realms? Lethaia, 41, 147-153.

Sheehan, P.M., 1988. Late Ordovician events and the terminal Ordovician extinction. New Mexico Bureau of Mines and Mineral Resources Memoirs. 44, 405–415.

Shields, G.A., Carden, G.A.F., Veizer, J., Meidla, T., Rong, J.-Y., Li, R.-Y., 2003. Sr, C, and O isotope geochemistry of Ordovician brachiopods: A major isotopic event around the Middle-Late Ordovician transition. Geochim. Cosmochim. Acta 67, 2005–2025. doi:10.1016/S0016-7037(02)01116-X

Skelton, P.W., 1994. Radiations and extinctions in the history of life: what turns the “wheel of fortune”? Eur. Palaeontol. Newsl. 6, 15–21.

Stanley, S.M., 1988. Paleozoic mass extinctions — shared patterns suggest global cooling as a common cause. Am. J. Sci. 288, 334–352.

Stanley, S.M., 2010. Thermal barriers and the fate of perched faunas. Geology 38, 31–34.

Stanley, S.M., 2007. An analysis of the history of marine animal diversity. Paleobiology 33, 1–55.

Stanley, S.M., Powell, M.G., 2003. Depressed rates of origination and extinction during the late Paleozoic ice age: a new state for the global marine ecosystem. Geology, 31, 877-880.

Stirling, C.H., Andersen, M.B., Potter, E.K., Halliday, A.N., 2007. Low-temperature isotopic fractionation of uranium. Earth Planet. Sci. Lett. 264, 208–225. doi:10.1016/j.epsl.2007.09.019

Stirling, C.H., Halliday, A.N., Porcelli, D., 2005. In search of live 247Cm in the early solar system. Geochim. Cosmochim. Acta69, 1059–1071

Telus, M., Dauphas, N., Moynier, F., Tissot, F.L.H., Teng, F.-Z., Nabelek, P.I., Craddock, P.R., Groat, L.A., 2012. Iron, zinc, magnesium and uranium isotopic fractionation during continental crust differentiation: The tale from migmatites, granitoids, and pegmatites. Geochim. Cosmochim. Acta 97, 247–265. doi:10.1016/j.gca.2012.08.024

Thual, O., Mcwilliams, J.C., 1992. The catastrophe structure of thermohaline convection in a two-dimensional fluid model and a comparison with low-order box models. Geophys. Astrophys. Fluid Dyn. 64, 67–95. doi:10.1080/03091929208228085

Tissot, F.L.H., Dauphas, N., 2015. Uranium isotopic compositions of the crust and ocean: Age corrections, U budget and global extent of modern anoxia. Geochim. Cosmochim. Acta 167, 113–143. doi:10.1016/j.gca.2015.06.034

Trotter, J.A., Williams, I.S., Barnes, C.R., Lécuyer, C., Nicoll, R.S., 2008. Did cooling oceans trigger Ordovician biodiversification? Evidence from conodont thermometry. Science (80-.). 321, 550–554. doi:doi:10.1126/science.1155814

Van Cappellen, P., Ingall, E.D., 1994. Benthic phosphorus regeneration, net primary production, and ocean anoxia: A model of the coupled marine biogeochemical cycles of carbon and phosphorus. Paleoceanography 9, 677–692.

Vandenbroucke, T.R., Armstrong, H.A., Williams, M., Paris, F., Zalasiewicz, J.A., Sabbe, K., Nõlvak, J., Challands, T.J., Verniers, J., Servais, T., 2010. Polar front shift and atmospheric CO2 during the glacial maximum of the Early Paleozoic Icehouse. Proceedings of the National Academy of Sciences. 107, 14983-14986.

Veizer, J., Goddéris, Y., Francois, L.M., 2000. Evidence for decoupling of atmospheric CO2 and global climate during the Phanerozoic eon. Nature 408, 698–701. doi:10.1038/35047044

Wang, K., Chatterton, B.D.E., Attrep Jr., M., Orth, C.J., 1993a. Late Ordovician mass extinction in the Selwyn Basin, northwestern Canada: geochemical, sedimentological, and paleontological evidence. Can. J. Earth Sci. 30, 1870–1880. doi:10.1139/e93-165

Wang, K., Orth, C.J., Attrep Jr., M., Chatterton, B.D.E., Wang, X., Li, J., 1993b. The great latest Ordovician extinction on the South China Plate: Chemostratigraphic studies of the Ordovician-Silurian boundary interval on the Yangtze platform. Palaeogeogr. Palaeoclimatol. Palaeoecol. 104, 61–79. doi:10.1016/0031-0182(93)90120-8

Weyer, S., Anbar, A.D., Gerdes, A., Gordon, G.W., Algeo, T.J., Boyle, E.A., 2008. Natural fractionation of 238U/235U. Geochim. Cosmochim. Acta 72, 345–359. doi:10.1016/j.gca.2007.11.012

Wickson, S., 2010. High-resolution carbon isotope stratigraphy of the Ordovician-Silurian boundary on Anticosti Island, Quebec: Regional and global implications. University of Ottawa.

Wignall, P.B., Myers, K.J., 1988. Interpreting benthic oxygen levels in mudrocks: A new approach. Geology 16, 452–455. doi:10.1130/0091-7613(1988)016<0452:IBOLIM>2.3.CO;2

Wilde, P., Berry, W.B.N., 1984. Destabilization of the oceanic density structure and its significance to marine “extinction” events. Palaeogeogr. Palaeoclimatol. Palaeoecol. 48, 143-162.

Worthington, L.V., 1968. Genesis and evolution of water masses. Meteorol. Monogr. 8, 63–67.

Yan, D., Chen, D., Wang, Q., Wang, J., 2012. Predominance of stratified anoxic Yangtze Sea interrupted by short-term oxygenation during the Ordo-Silurian transition. Chem. Geol. 291, 69–78. doi:10.1016/j.chemgeo.2011.09.015

Yapp, C.J., Poths, H., 1992. Ancient atmospheric C02 pressures inferred from natural goethites. Nature 355, 342–344. doi:10.1038/355342a0

Zhang, T., Yanan, S., Zhan, R., Shen, S., Chen, X., 2009. Large perturbations of the carbon and sulfur cycle associated with the Late Ordovician mass extinction in South China. Geology 37, 299–302. doi:10.1130/G25477A.1